



AMERICAN UNIVERSITY OF BEIRUT

TRANSIENT STABILITY ANALYSIS OF GRID  
CONNECTED WIND TURBINES EMPLOYING INDUCTION  
GENERATORS

by  
ANIS JAMIL HAZIMEH

A thesis  
submitted in partial fulfillment of the requirements  
for the degree of Master of Engineering  
to the Department of Electrical and Computer Engineering  
of the Faculty of Engineering and Architecture  
at the American University of Beirut

Beirut, Lebanon  
January 2013

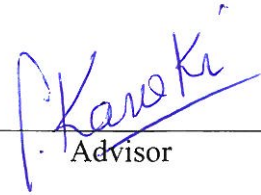
AMERICAN UNIVERSITY OF BEIRUT

TRANSIENT STABILITY ANALYSIS OF GRID  
CONNECTED WIND TURBINES EMPLOYING INDUCTION  
GENERATORS

by  
ANIS JAMIL HAZIMEH

Approved by:

Prof. Sami Karaki, Professor  
Electrical and Computer Engineering

  
Advisor

Prof. Riad Chedid, Professor  
Electrical and Computer Engineering

  
Member of Committee

Prof. Rabih Jabr, Associate Professor  
Electrical and Computer Engineering

  
Member of Committee

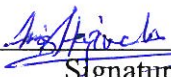
Date of thesis defense: [January 15, 2013]


AMERICAN UNIVERSITY OF BEIRUT

THESIS RELEASE FORM

I, Anis Jamil Hazimeh

- authorize the American University of Beirut to supply copies of my thesis/dissertation/project to libraries or individuals upon request.
- do not authorize the American University of Beirut to supply copies of my thesis/dissertation/project to libraries or individuals for a period of two years starting with the date of the thesis/dissertation/project defense.

  
Signature

  
Date

## ACKNOWLEDGMENTS

First and foremost, I thank GOD for His great blessings, which allowed me to confront all the challenges that I faced throughout this research. I sincerely believe that His existence in my life has provided me with the strength to persist and the hope to aspire.

I seize this opportunity to express my very deep appreciation and gratitude to Prof. Sami Karaki for his continuous guidance and support throughout this project. This work could have been much more complicated without his helpful instructions and bright ideas.

I would also like to thank the committee members, Prof. Riad Chedid and Prof. Rabih Jabr, for their assistance in specifying my thesis objectives and rendering its implementation possible within the available time span.

Finally, I would like to dedicate this work to my beloved family and friends who stood by me and encouraged me during my hard times. I would like to thank my mom and dad for the endless care and love they overwhelmed me with, and for their support and frequent prayers. You are the main reason for me being at this point in my life.

# AN ABSTRACT OF THE THESIS OF

Anis Jamil Hazimeh for Master of Engineering  
Major: Electrical and Computer Engineering

Title: Transient Stability Analysis of Grid Connected Wind Turbines Employing Induction Generators

The number of grid connected wind turbines has been recently in a continuous growth. Therefore, it becomes extremely essential to analyze the transient stability of power systems with these new units. In this thesis, the transient stability of fixed speed wind turbines is investigated. A power flow algorithm is established to provide the necessary initial conditions for the dynamic simulation. The transient machine models are presented further together with their comprehensive initialization and integration techniques. These comprise the synchronous machine two-axis model, the AVR excitation system model, and the wind turbine electrical and mechanical system models. The validity of the proposed models is verified by a transient stability program that is developed in MATLAB and used to perform a case study on the 220/150 KV Lebanese network with a wind farm. In this study a three phase fault is simulated and the machine angles along with the turbine speeds are noted. Simulations show that a one mass model doesn't adequately represent the oscillatory response of a windmill in contrast to a two mass model. The former yields optimistic results in terms of the critical clearing time, which in turn is affected by the reactive power consumption, the fault location, the penetration level and the machine parameters.

# TABLE OF CONTENTS

ACKNOWLEDGEMENTS.....	v
ABSTARCT.....	vi
LIST OF ILLUSTRATIONS.....	x
LIST OF TABLES.....	xii
Chapter	
1. INTRODUCTION.....	1
1.1. Wind Energy and the Transient Stability Problem.....	1
1.2. Wind Turbine Generator Types.....	2
1.3. Literature Review.....	4
1.4. Thesis Contribution.....	8
1.5. Thesis Organization.....	9
2. WIND TURBINE MODELS FOR LOAD FLOW ANALYSIS.....	10
2.1. Modeling a Wind Turbine Generating Unit.....	10
2.1.1. Wind Turbine Output Power.....	11
2.1.2. Wind Turbine Characteristic Curves.....	12
2.1.2.1. Performance Coefficient Characteristic Curves.....	12
2.1.2.2. Power versus Angular Speed Characteristic Curves	13
2.1.2.3. Wind Turbine Power Curve.....	14
2.2. Literature Survey on Wind Turbine Power Flow Models.....	15
2.3. The Implemented Power Flow Algorithm.....	16

2.3.1. Wind Turbine Generator Model.....	17
2.3.2. Power Flow Algorithm with Grid-Connected Wind Turbines	20
2.4. Summary.....	22
<b>3. SYNCHRONOUS MACHINE AND WIND TURBINE MODELING IN TRANSIENT STABILITY STUDIES...</b>	<b>23</b>
3.1. Mechanical Dynamics of a Synchronous Machine.....	23
3.2. Synchronous Machine Electrical Equations.....	27
3.2.1. Classical Synchronous Machine Model.....	28
3.2.2. Two Axis Synchronous Machine Model.....	28
3.3. Automatic Voltage Regulator.....	35
3.4. Wind Turbine Dynamic Modeling.....	38
3.4.1. Mechanical Model of a Wind Turbine.....	38
3.4.1.1. The Rotor Model.....	38
3.4.1.2. The Shaft Model.....	39
3.4.2. Induction Machine Transient Model.....	42
3.5. Structure of a Transient Stability Program.....	44
3.6. Initialization Scheme and the Implicit Trapezoidal Method.....	46
3.6.1. Initial Conditions.....	46
3.6.1.1. Synchronous Machine Initial Conditions.....	46
3.6.1.2. AVR Initial Conditions.....	46
3.6.1.3. Wind Turbine Initial Conditions.....	47
3.6.2. The Implicit Trapezoidal Method.....	47
3.7. Summary.....	51
<b>4. WINDMILL MODEL VALIDATION RESULTS AND A CASE STUDY ON THE LEBANESE POWER SYSTEM.....</b>	<b>52</b>
4.1. Wind Turbine Model Validation Results.....	52



4.1.1. Wind Turbine Load Flow Results.....	53
4.1.2. Wind Turbine Transient Stability Results.....	55
4.2. A Case Study on the Lebanese Power System with a Wind Park.....	60
4.2.1. Simulation Model and Results.....	65
4.2.1.1. Case 1.....	67
4.2.1.2. Case 2.....	70
4.2.1.3. Case 3.....	71
4.3. Summary.....	72
5. CONCLUSION AND FUTURE WORK.....	73
APPENDIX 1.....	75
1. Line and Machine Data.....	75
BIBLIOGRAPHY .....	78

# ILLUSTRATIONS

## Figure

2.1. Performance coefficient curves .....	12
2.2. Power output as a function of turbine speed .....	13
2.3. Power curves for a stall regulated (dotted), and a pitch controlled wind turbine	14
2.4. SCIG exact equivalent circuit .....	17
2.5. SCIG power slip curve .....	19
2.6. Wind farm aggregate circuit .....	21
3.1. Synchronous generator angles in space .....	24
3.2. Phasor diagram of a salient pole synchronous machine in the steady-state.....	29
3.3. Synchronous machine and network frames of reference .....	30
3.4. Phasor diagram of a synchronous machine in the transient state .....	31
3.5. Machine transient equivalent circuits .....	32
3.6. Adjusted Norton equivalent circuit .....	34
3.7. IEEE Type 1 excitation system model .....	35
3.8. Two mass model representation .....	41
3.9. Induction machine circuit in the transient state .....	42
4.1. Active power generation and reactive power consumption at the terminals of a SCIG as a function of the slip and voltage .....	54
4.2a. One mass model transient response with a fault clearing time of 349 ms .....	56
4.2b. One mass model transient response with a fault clearing time of 350 ms .....	56
4.3a. Two mass model transient response with a fault clearing time of 119.23 ms ....	57
4.3b. Two mass model transient response with a fault clearing time of 119.23 ms ....	57
4.4. 3 MW SCIG torque slip characteristics .....	59

4.5. The Lebanese power system .....	61
4.6. Weibull distribution for Akkar at a height of 90 m .....	64
4.7. One Line Diagram of the 150/220 KV transmission network with bus numbers	65
4.8a. Wind farm transient response without a capacitor bank. CT: 84 ms .....	67
4.8b. Synchronous machines transient response without a capacitor bank. CT: 84 ms	67
4.9a. Wind farm transient response with a capacitor bank. CT: 84 ms .....	68
4.9b. Synchronous machines transient response with a capacitor bank. CT: 84 ms ..	68
4.10. Wind farm transient response with a capacitor bank. CCT: 140 ms .....	70
4.11a. Wind farm transient response with a capacitor bank. CT: 140 ms .....	71
4.11a. Synchronous machines transient response with a capacitor bank. CT: 140 ms	71

## TABLES

### Table

1.1. Fixed speed versus variable speed wind turbines.....	3
2.1. Asynchronous Machine Data on 100MVA system Bas .....	19
4.1. The Proposed PQ Model Load Flow Results.....	53
4.2. Wind turbine infinite bus system data.....	55
4.3. Thermal Power Plants in Lebanon .....	62
4.4. Wind Speed Ranges in m/s and Their Probabilities at a Height of 16 m.....	62
4.5. Wind Speed Ranges in m/s and Their Probabilities at a Height of 90 m.....	63
4.6. Weibull Parameters for Akkar at a Height of 90 m.....	64

# CHAPTER 1

## INTRODUCTION

In recent years, the generation of electric energy from wind has comprised one of the fundamental objectives of several electric utilities worldwide. This is primarily due to the depleting nature of fossil fuel energy sources, and their adverse environmental effects. Wind energy, to start with, is one of the most safe and clean renewable energy sources. It possesses the highest conversion efficiency, and it is understood to be the most cost competitive among all the available renewable energy sources [1]. As a result, increasing numbers of wind turbines are being integrated with the grid to provide new solutions for the growing energy demands, and mitigate the dependence on unsustainable energy sources. However, the increased penetration of these new generating units leads to concerns about their effects on the transient stability of power systems following a particular disturbance.

### **1.1 Wind Energy and the Transient Stability Problem**

The increased penetration of wind energy conversion devices could significantly deteriorate the power system stability. For instance, a large disturbance such as a fault may occur and cause the wind turbines to lose their stability. This in turn will prevent the turbines from generating active power and converts them to loads, which only consume reactive power. Under such conditions, the voltage at the relevant nodes will sag and a voltage stability problem arises. To prevent this, grid operators urge the disconnection of the windmills to protect the network against the voltage fluctuations. This protection technique is possible when the installed wind capacity is

very small. But when the wind power becomes appreciable, the protective disconnection turns out to be impractical. Since this will lead to a considerable loss of generation that will threaten the power system stability. As a result, system operators are imposing severe requirements on the integration of wind turbines, where these devices should remain connected during a transient fault period and keep the system stable. For these reasons, it becomes of extreme importance to study the transient stability of power systems with these new units.

## **1.2 Wind Turbine Generator Types**

Transient stability analysis requires appropriate modeling of wind energy conversion devices. Different models yield different dynamic responses, hence affecting the transient behavior of the power system. Wind turbine systems are either equipped with induction generators or synchronous ones. Induction generators are favorable due to their rugged construction, simple operation, and low maintenance cost. Also their torque slip curve can handle the variability of the resource by maintaining the system frequency at a different rotor frequency. They are primarily classified as fixed speed or variable speed generators. Fixed speed induction generators (FSIG) use squirrel cage rotors. They are termed as fixed speed since their torque-slip curve is very steep, which renders any change in speed very small in magnitude. Their speed is determined by the grid frequency, the gearbox, and the generator's characteristics. These generators are directly connected to the grid and draw their reactive power from it. Doubly fed induction generators (DFIG) use wound rotors and are characterized by their variable speed operation. They are known as doubly fed because their rotors permit an external connection to the grid through a back-to-back variable frequency power converter. This

allows the control of the turbine's speed through decoupling the mechanical rotor frequency and the electrical grid frequency. The table below summarizes the advantages and disadvantages of each of the mentioned turbine types.

Table 1.1: Fixed speed versus variable speed wind turbines  
Sources:[1,2]

	<b>Wind Turbines with FSIG</b>	<b>Wind Turbines with DFIG</b>
<b>Advantages</b>	Cheap and robust	Controllability of active and reactive power
	Less maintenance due to its simple construction	Fewer fluctuations in output power due to large rotor inertia
	Electrically efficient	Aerodynamically efficient
	Lack of harmonics that result from frequency conversion	Less mechanical stress
	Lack of active and reactive power control	Complex control strategies
<b>Disadvantages</b>	Aerodynamically less efficient	Expensive
	Gearbox breakdown that result from torque pulsations	Electrically less efficient

In this research we will limit our study to squirrel cage induction generators (SCIG), since there is a large number of grid connected wind turbines that employ this type. Furthermore, the doubly fed induction generator (DFIG) is equipped with a crowbar protection. The latter imposes a short circuit on the rotor bars upon its activation. Under this condition, the dynamic behavior of the DFIG during a transient period resembles that of a SCIG. Therefore, it becomes essential to investigate the performance of fixed speed wind turbines even in the presence of variable speed turbines.

### 1.3 Literature Review

Several papers have been published in the literature addressing the effects of wind turbines on the electrical grid. Transient stability also known as rotor angle stability, has gained a considerable amount of attention in recent years. This is attributed to the rapid development and high penetration of wind energy conversion systems. Authors in this field have dealt with both squirrel cage and doubly fed induction generators.

The transient behavior of fixed speed wind turbines has been widely considered in the literature. Some authors have focused on the modeling of wind turbines and the effects of different drive train models on transient stability. They have also studied the influence of various electrical and mechanical parameters on the critical clearing time [3-9]. While others have proposed different methods for the dynamic equivalence of wind turbines within a particular wind farm [10-13].

In [3], a comparison between the different drive train models for transient stability analysis has been performed. The two-mass shaft model appears to be the most suitable, since it provides reasonable accuracy in demonstrating the oscillations of various operational parameters (voltage, current, active power, reactive power, and speed). In this case, one mass represents the rotor of the turbine and the second is the rotor of the generator. The mass of the gearbox is incorporated with either the turbine's rotor or the generator's rotor depending on the stiffness of the low speed and high speed shafts. For instance, if the stiffness constant of the low speed shaft is smaller than that of the high speed shaft, then the gearbox inertia will be added to the generator's inertia.

Salman *et al* in [4] examine the effect of different shaft models on the critical clearing time. They show that a one-mass model cannot accurately explain the transient



behavior of a windmill. This is due to the fact that a lumped mass model yields a larger critical clearing time than that of the shaft models and provides fewer oscillations. They also conduct other studies to determine the factors that improve the stability.

Simulations signify that a higher critical clearing time can be obtained through a larger moment of inertia, increased shaft stiffness, and an improved power factor.

In [7], the transient behavior of various wind turbine models has been studied along with their effect on the critical clearing time. A 5<sup>th</sup> order wind turbine model proves to be adequate in evaluating the dynamic performance of a wind generator. In this model, the induction generator is represented by the 2<sup>nd</sup> order transient state machine model. The stator transients are neglected since they're very fast as compared to the rotor dynamics. The mechanical drive system incorporates a two-mass model.

Jurado *et al* in [8] clarify that it is essential to adopt a two-mass model in wind turbine transient stability studies. This is true since a lumped mass model cannot predict the actual perturbations of the turbine's speed, voltage, active and reactive power during a disturbance. Their study inspects the significance of reactive power compensation as well. They show that static capacitors can assist the voltage recovery at the terminals of the wind farm when switched after fault clearance.

In [9], the transient stability of a fixed speed wind park is analyzed by determining the effects of different parameters on the critical clearing time. A 5<sup>th</sup> order wind turbine model has been implemented. Results show that the short circuit power has a strong effect on the critical clearing time at weak buses, while reactive power compensation has slighter effects. The system is more stable when the fault point is far from the wind farm, and the increase in distance varies linearly with the critical clearing

time. The rotor inertia also contributes to the stability, where larger masses decrease the acceleration and enhance stability.

References [10-13] deal with the aggregation of multiple wind turbines within a wind park. These propose that the entire wind farm can be aggregated into one equivalent windmill when the wind velocity is similar across the entire area. While if the wind is irregular, multiple wind turbines experiencing the same incoming wind speed can be grouped into one equivalent machine.

References [14-17] analyze the impact of different wind turbine penetration levels on transient stability and suggest improvement techniques through using reactive power compensation and pitch control. Authors in [14] have replaced a part of the synchronous generator units with windmills and determined the acceptable wind power penetration level, which will keep the system stable. They have also studied the influence of static VAR compensation on transient stability.

Tamura *et al* in [17] analyze the simulation results of a transient stability study of a grid-connected wind farm. They highlight the importance of the pitch controller through its vital role in enhancing the dynamic performance of the wind generator. The pitch controller limits the turbine's acceleration during the fault period, hence rendering the voltage recovery faster upon fault clearance. This is attributed to the fact that the reactive power consumption of a SCIG is proportional to the slip. Hence, upon fault clearance the turbine would have been accelerated under the action of imbalance between the mechanical input torque and the electromagnetic torque. As a result the SCIG consumes additional reactive power from the grid, which in turn may dip the voltage at the machine terminals.

Doubly fed induction generators (DFIG) have been broadly explored in the literature. This is due to their advantages over squirrel cage induction generators (SCIG) in terms of their various control and operational features. Authors in this field have proposed different models for this type of generators, which are suitable for transient stability studies [18-21]. Others have studied the influence of grid-connected wind energy conversion devices on the transient stability of the power system, where a comparison has been carried out between SCIG's and DFIG's in an attempt to determine the more convenient type [21-23].

In [18], the authors propose a model of the DFIG suitable for transient stability analysis. Electromagnetic transients in the stator are neglected as well as the dynamics of current control loops of the converters. The DFIG is modeled by a set of 15 static algebraic equations. These are solved by an iterative procedure with the static equations existing in the power flow program. The solution of the entire set of equations provides the initial conditions for the transient stability program. A detailed windmill model is then introduced, where it incorporates the proposed DFIG model in addition to the models of the mechanical system, the dc-link, the dc-voltage control system, the wind torque, and the speed control systems. The resulting model is tested and the obtained results prove its feasibility.

In [19], a reduced order dynamic model for the DFIG and its associated protection and control circuits has been developed. Simulations evince that stability can be improved by properly selecting the proportional gain of the speed and reactive power controllers. In [20] several reduced order models for the DFIG have been tested. Results prove that a 3<sup>rd</sup> order machine model equipped with crowbar protection together with a simplified model of the converter is sufficient to provide acceptable accuracy in

transient stability studies for a large power system. Control concepts for the generator and turbine have been also explored.

The authors in [21] investigate the effect of both the SCIG and the DFIG on the transient stability of the Southern Italy Power System when a substantial number of wind generators are available. Suitable mathematical models for both machines are analyzed and compared. Both employ a 3<sup>rd</sup> order model in addition to their corresponding control systems. The influence of both types on the rotor angle stability of synchronous generators has been studied. Each synchronous machine adopts a 9<sup>th</sup> order model that comprises the equations governing the dynamics of the machine, in addition to a 2<sup>nd</sup> order excitation system model, and a 3<sup>rd</sup> order model for the speed governor. Results point out to an improvement of the global stability of the system when DFIG's are deployed.

#### **1.4 Thesis Contribution**

The contribution of this work lies in developing a transient stability program that studies the dynamic behavior of fixed speed wind turbines under a disturbance. Future plans are currently being set in Lebanon to install wind turbines. Hence it becomes essential at the planning level to study the transient stability of the system with these units prior to their installation. As a result, a case study will be performed on the Lebanese power system to investigate the influence of fixed speed wind turbines on the global stability of the system. The effect of different parameters on the critical clearing time will be analyzed in order to site the sources that may deteriorate the system's stability.

## **1.5 Thesis Organization**

Following the introductory chapter, the thesis is organized as follows: Chapter 2 provides an introductory part, which reviews the physical basics of wind turbine modeling. The remaining sections introduce some models for wind turbines in power flow studies, and discuss the adopted algorithm. Chapter 3 deals with synchronous machine modeling for transient stability, and describes the implemented excitation system model. It also explains the fixed speed wind turbine dynamic model, and illustrates the complete algorithm for solving the transient stability problem using the implicit trapezoidal method. Chapter 4 includes the model validation results, and presents the simulations of the Lebanese power system. Finally, Chapter 5 concludes the thesis and points out at future developments in the current models.

## CHAPTER 2

### WIND TURBINE MODELS FOR LOAD FLOW ANALYSIS

Load flow analysis constitutes a major part in transient stability studies, as it provides the initial conditions of the network prior to a disturbance. Wind turbine modeling in power flow studies has been examined in detail. Several models have been proposed in an attempt to determine the windmill steady state parameters and initialize the dynamic simulation properly. This chapter gives an insight on some of the suggested power flow algorithms in the literature, and presents the model initialization procedure, which has been implemented in this research. An introductory section is present to explain the physical basics of wind turbine modeling.

#### **2.1 Modeling a Wind Turbine Generating Unit**

A wind turbine generating unit captures the kinetic energy in the flowing air particles and converts it into rotational energy in its rotor. The rotational energy is further converted through the transmission shaft, the gearbox, and the generator to electrical energy that feeds the grid. The proportion of the generated power is based on various factors such as the wind velocity, the size of the turbine, the rotor's angular speed, and the characteristics of the electric generator. Hence, a mathematical model that involves the specified parameters is necessary to understand the behavior of the windmill [1]. This section introduces the power and speed relationships, which govern the operation of a wind turbine.

### 2.1.1 Wind Turbine Output Power

The mechanical power extracted by a wind turbine depends on the rotor's swept area, the density of surrounding air, the performance coefficient, and the wind velocity in particular. The rotor's swept area is determined by the length of the blades. The density and speed of the incoming wind are resource dependent. They are affected by the terrain's altitude, humidity, and temperature. The performance coefficient, which is also known as the power coefficient represents the fraction of wind power that the rotor blades capture and transmit to the generator. The magnitude of this coefficient varies during the turbine's operation based on the wind velocity, the blades rotational speed, and the aerodynamic characteristics. The theoretical maximum of the power coefficient is specified by Betz limit. Betz criterion states that it is physically impossible to exploit more than 59.3 percent of the power available in a wind stream [24]. Practical wind turbines can harness up to 40 percent of the accessible wind power.

The following expression shows how the extracted mechanical power relates the described variables together:

$$P_m = \frac{1}{2} \rho A_R v^3 C_p(\lambda, \theta) \quad (2.1)$$

$$\lambda = \frac{\omega_r R}{v} \quad (2.2)$$

Where,  $\rho$  is the air density in  $\text{Kg/m}^3$ ,  $A_R$  is the rotor's swept area in  $\text{m}^2$ ,  $v$  is the undisturbed wind velocity in  $\text{m/sec}$ , and  $C_p$  is the performance coefficient. The power coefficient is expressed in terms of the pitch angle  $\theta$  in degrees, and the tip speed ratio  $\lambda$ . The latter is a function of the rotor's radius  $R$  in meters, the rotor's angular speed  $\omega_r$  in  $\text{rad/sec}$ , and the wind velocity.

### 2.1.2 Wind Turbine Characteristic Curves

The following curves are used to demonstrate the power and speed characteristics, which govern the operation of a wind turbine.

#### 2.1.2.1 Performance Coefficient Characteristic Curves

The mechanical power of a wind turbine can be controlled by varying the value of the performance coefficient  $C_p$  through changing the tip speed ratio  $\lambda$ , or the pitch angle  $\theta$ . Wind turbine manufacturers usually provide  $C_p(\lambda, \theta)$  curves for a particular wind generating unit. These curves do not differ significantly among different turbines, and previous numerical techniques have been developed to approximate them. Man *et al* in 1981 proposed the following expression [25]:

$$C_p(\lambda, \theta) = c_1 \left( \frac{v}{\omega_r} - c_2\theta - c_3\theta^n - c_4 \right) e^{-\frac{v}{\omega_r}c_5} \quad (2.3)$$

Where  $c_1$  to  $c_5$  are coefficients specific to each wind turbine. The figure below depicts the power coefficient curves for a 3-bladed 60 m rotor, 1.2 MW turbine (WKA-60).

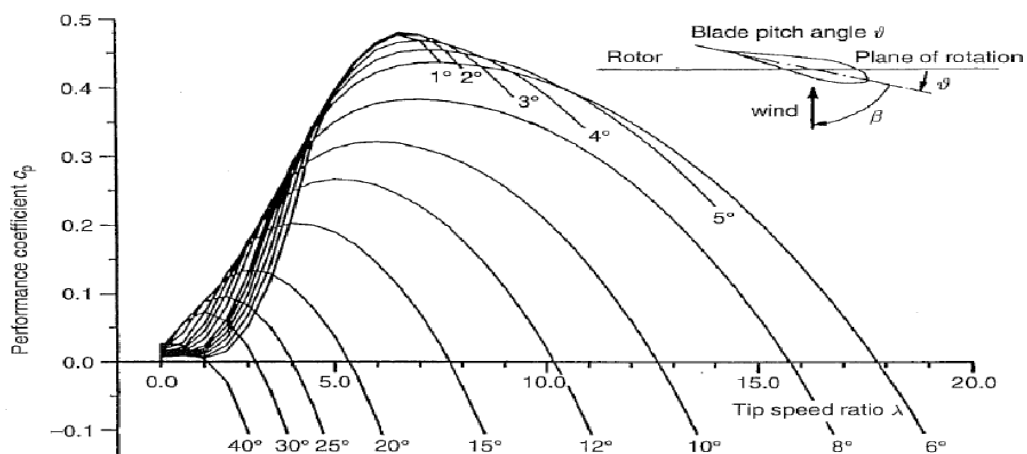


Fig 2.1: Performance coefficient curves  
Source: [25]



### 2.1.2.2 Power versus Angular Speed Characteristic Curves

The analytical expression of the power coefficient curve can be combined with the mechanical power equation to obtain the power-angular speed characteristics of a wind turbine ( $P_m$  versus  $\omega_r$ ). Hence, at a given pitch angle, the curves are as follows:

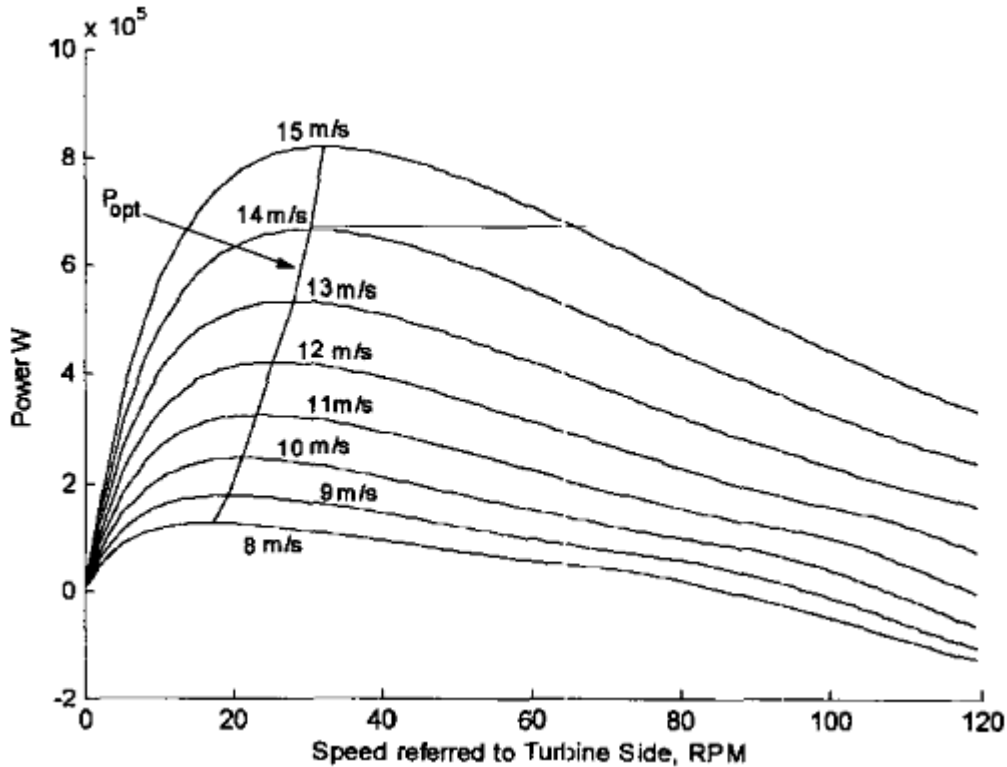


Fig 2.2: Power output as a function of turbine speed  
Source: [26]

The curves in Fig. 2.2 depict the variation of the turbine's output power with the rotor's angular speed at a specific pitch angle. Thus at each wind speed a large number of curves can be obtained corresponding to different pitch angles. This will be the case when the turbine is equipped with a pitch controller. The curves above apply to stall regulated windmills, which have a constant pitch angle.

### 2.1.2.3 Wind Turbine Power Curve

The power curve of a wind turbine provides data about the amount of electric power it can generate at a specific wind speed. The graph below shows the power curves for a stall and a pitch controlled wind turbine:

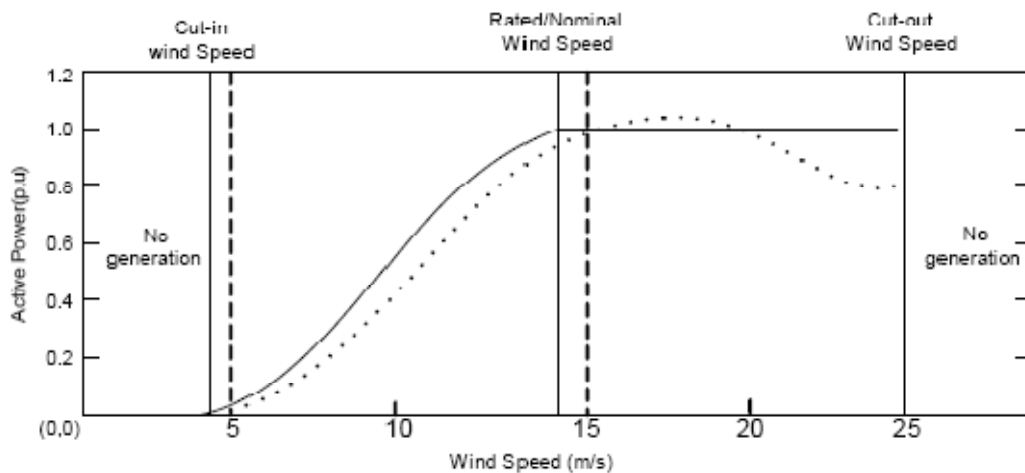


Fig 2.3: Power curves for a stall regulated (dotted), and a pitch controlled wind turbine  
Source: [2]

In a pitch controlled wind turbine, the generated electric power becomes constant above the nominal wind speed, so as to match the generator's rating. The power level is kept constant by the action of the pitch controller that lowers the value of  $C_p$ . Whereas, in a stall regulated wind turbine the power level peaks at some point and then drops down. This is attributed to the aerodynamic characteristics of the turbine. Based on the blade element theory, when the wind velocity increases, the angle of attack increases because the angular speed is approximately constant in a fixed speed wind turbine. Therefore the lift coefficient decreases, and lowers the aerodynamic efficiency, which in turn will cause a drop in the power level.

## 2.2 Literature Survey on Wind Turbine Power Flow Models

Several researchers have investigated the interaction between the grid and the wind turbine generating units during steady state. In [27-28], two models for load flow analysis have been proposed based on the steady state equivalent circuit of the squirrel cage induction machine. The first model represents the wind turbine by a conventional PQ bus. In this condition, the injected active power at a given wind speed is obtained from the turbine's power curve. The reactive power is either calculated according to a specified power factor, or is expressed as a function of the terminal voltage. In the first case, the active and reactive powers remain constant throughout the load flow analysis. While in the other, the reactive power is updated in each iteration. In the second model, the wind turbine is modeled as an RX node. At a given slip, the machine impedance is calculated and the load flow program is run. This procedure is repeated until the machine's operating slip is determined by the turbine and generator characteristic curves. Thus, two iterative processes take place: one for the load flow solution and another for the slip calculation. Simulations indicate that the two proposed models yield acceptable results, but the second one is very exact despite its computational complexity.

Divya *et al* in [29] differentiate between the models of stall regulated and pitch controlled wind turbines. In the case of a stall regulated unit, it is inaccurate to use the power curve for determining the active power injection. In fact, the turbine's power curve yields the output electric power at a particular wind speed without taking into account the electrical network conditions. In other words, if the voltage varies at the terminals of the induction machine, the developed power will differ and result in a mismatch with the turbine's mechanical input power. Thus, it becomes essential to

match the turbine's power-speed characteristics with those of the generator before computing the active power injection. This can be done by adopting the RX model in [27-28]. In this paper, a more efficient method is proposed with a less computational effort. Concerning pitch controlled units; the power curve is used to determine the active power injection at a PQ node. In this context, the pitch controller can always maintain a constant electrical power output at a certain wind speed regardless of the network conditions. Therefore, the power curve is the only required input for this model.

In [30], a power flow algorithm is proposed based on the PQ model of pitch controlled wind turbines. The active power is an input variable that remains constant, while the reactive power is rectified in every iteration of the power flow solution depending on the generator's voltage and slip. A quadratic equation relates the generator's slip to the node voltage and active power. This is derived from the induction machine approximate equivalent circuit. Simulations indicate that the proposed algorithm is reliable and possesses a high practical value.

### **2.3 The Implemented Power Flow Algorithm**

In this research, the windmill is modeled as a PQ node in load flow studies. The turbine's electric output power is derived from the power curve, and is kept constant throughout the load flow analysis. The reactive power is modified in every iterative process in accordance with the terminal voltage and slip. Hence, this model resembles the one applied in reference [30], however the exact equivalent circuit of the induction machine is used. Besides, the load flow problem is solved using the fast-

decoupled method. In what follows, the derived mathematical relations are introduced and the solution steps are explained.

### 2.3.1 Wind Turbine Generator Model

The exact equivalent circuit of an induction machine in its generating state is shown in Fig 2.4.  $R_1$  is the stator resistance;  $X_1$  is the stator reactance;  $R_2$  is the rotor resistance referred to the stator's side;  $X_2$  is the rotor reactance referred to the stator's side;  $X_m$  is the magnetizing reactance;  $s$  is the slip; it is a negative quantity.

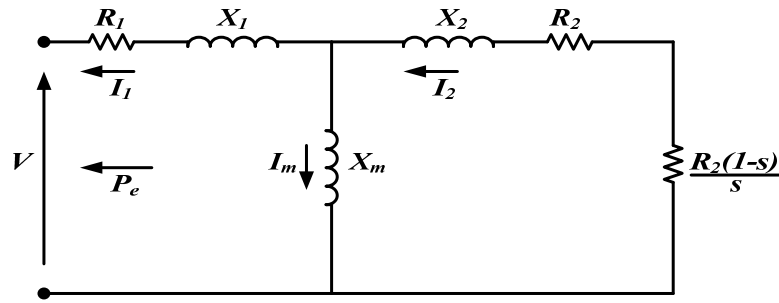


Fig 2.4: SCIG exact equivalent circuit

The rotor and stator currents are given by:

$$\vec{I}_1 = \frac{\vec{V}}{Z_{eq}} \quad (2.4)$$

$$\vec{I}_2 = \vec{A} \vec{I}_1, \text{ where } \vec{A} = \frac{jX_m}{\frac{R_2}{s} + j(X_1 + X_2)} \quad (2.5)$$

The grid-injected electrical power  $P_e$ , is determined from the turbine's power curve at a specific wind speed. It relates to the above circuit by the following relation

$$-\frac{|\vec{I}_2|^2 R_2 (1-s)}{s} - |\vec{I}_2|^2 R_2 - |\vec{I}_1|^2 R_1 = P_e \quad (2.6a)$$

which is equivalent to:

$$-\frac{|\vec{I}_2|^2 R_2}{s} - |\vec{I}_1|^2 R_1 = P_e \quad (2.6b)$$

Replacing the currents  $\vec{I}_1$  and  $\vec{I}_2$  with their quantities in equations (2.4) and (2.5) gives:

$$-\left|\frac{\vec{V}}{Z_{eq}}\right|^2 \left[|\vec{A}|^2 \frac{R_2}{s} + R_1\right] = P_e \quad (2.6c)$$

Equations (2.6a) to (2.6c) account for the power transfer in an induction generator. The first term in (2.6a) is the developed electrical power, and it is equal to the turbine's mechanical power. The second and third terms are the rotor and stator copper losses respectively. The machine equivalent impedance is denoted by  $Z_{eq}$  and is expressed as:

$$\vec{Z}_{eq} = \frac{\left(\frac{R_2}{s} + jX_2\right)jX_m}{\frac{R_2}{s} + j(X_2 + X_m)} + R_1 + jX_1 \quad (2.7a)$$

$$\vec{Z}_{eq} = \frac{\left(\frac{R_1 R_2}{s} - X_2 X_m - X_1 X_m - X_1 X_2\right) + j\left(\frac{R_2}{s} X_m + \frac{R_2}{s} X_1 + R_1 X_2 + R_1 X_m\right)}{\frac{R_2}{s} + j(X_2 + X_m)} \quad (2.7b)$$

By substituting equations (2.5) and (2.7b) in (2.6c), a quadratic equation in terms of the slip will be obtained with the resulting coefficients:

$$as^2 + bs + c = 0 \quad (2.8)$$

$$a = \left( X_2^2 X_m^2 + X_1^2 X_m^2 + X_1^2 X_2^2 + 2X_1 X_2 X_m^2 + 2X_1 X_m X_2^2 + 2X_2 X_m X_1^2 + R_1^2 X_1^2 \right. \\ \left. + R_1^2 X_m^2 + 2X_2 X_m R_1^2 + \frac{|\vec{V}|^2 (X_2 + X_m)^2 R_1}{P_e} \right) P_e \quad (2.8a)$$

$$b = 2R_1 R_2 X_m^2 P_e + |\vec{V}|^2 R_2 X_m^2 \quad (2.8b)$$

$$c = \left( \frac{|\vec{V}|^2 R_1 R_2^2}{P_e} + R_1^2 R_2^2 + R_2^2 X_m^2 + R_2^2 X_1^2 + 2X_1 X_m R_2^2 \right) P_e \quad (2.8c)$$

Equation (2.8) yields two values for the slip. The smaller quantity is always chosen since it makes up the stable part of the machine's torque-slip curve, while the other value is the one that supersedes the maximum pull-out torque. This is demonstrated by the following example, in which the slip expression in is used to plot the characteristics of a typical induction machine:

Table 2.1: Asynchronous Machine Data on 100MVA system Base  
Source: [31]

$R_1$	$X_1$	$R_2$	$X_2$	$X_m$	$V$ [p.u]
0.00571	0.06390	0.00612	0.18781	2.78	1.1

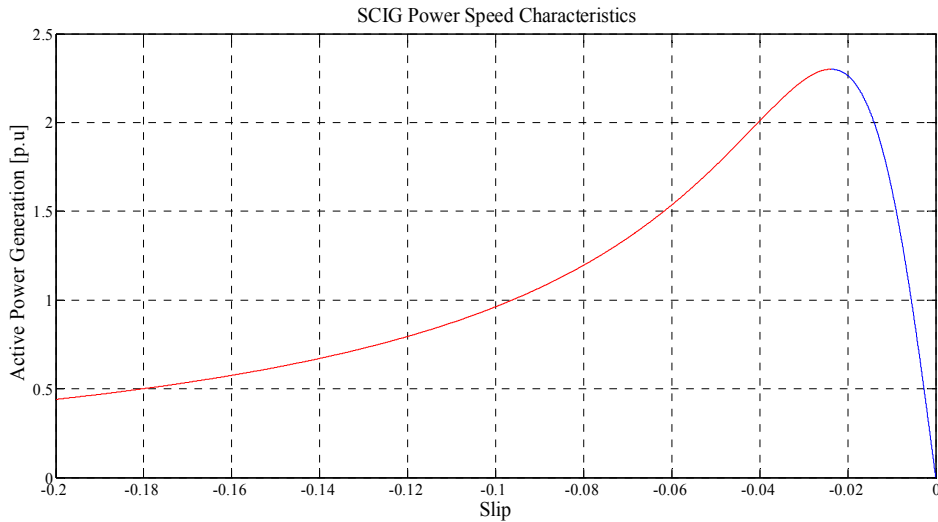


Fig 2.5: SCIG power slip curve

Figure 2.5 shows the power-slip curve of an induction machine in its generating state. The smaller root of equation (2.8) has been used to plot the blue part of the curve, whereas the larger one has produced the red portion of the graph. The same figure has been also obtained by plotting the machine's characteristics in a traditional

manner. In this sense, the slip is varied over a certain range and the output active power is computed correspondingly. This fact confirms the validity of the proposed model, which can be finalized by determining the value of the reactive power from:

$$Q_e = \text{Imaginary} \left( \vec{V} \vec{I}_1^* \right) \quad (2.9)$$

The described mathematical model is integrated in the power flow scheme. It is important to note that all the variables are expressed in per-unit and the stated equations (2.4 to 2.9) have been derived accordingly. In what follows, the solution steps of the load flow problem are outlined.

### ***2.3.2 Power Flow Algorithm with Grid-Connected Wind Turbines***

The comprehensive load flow solution is summarized in the following steps:

- Determine the electrical power output of a unit  $i$  using the power curve.
- Calculate the slip using equations (2.8, 2.8a to 2.8c). The voltage is equal to 1.0 p.u during the first iteration.
- Compute  $Z_{eq}$  and  $I_1$  using equations (2.7a) and (2.4).
- Find the reactive power injection from equation (2.9).
- Calculate the total active and reactive power injections of a wind farm by multiplying the individual injections by the number of turbines within a wind park. The wind speed is assumed constant across the entire farm.
- Calculate the active and reactive power mismatches using input node data.

Note that the wind farm nodes are characterized by PQ buses with no generating injections. In other words, the generated  $P$  and  $Q$  are equal to zero in the node data at the corresponding nodes.



- Include the calculated active and reactive power injections of the wind farms in the mismatch equations at the relevant nodes.
- Solve the correction equations to obtain new values for the nodal voltages and angles using the inverse of the Jacobian matrix.
- Perform a convergence check on the mismatch equations. If the mismatch is greater than “ $\epsilon$ ”, return to step 2.

An alternative way to include the wind farm in the above routine would be by modeling it by an equivalent windmill having the following circuit:

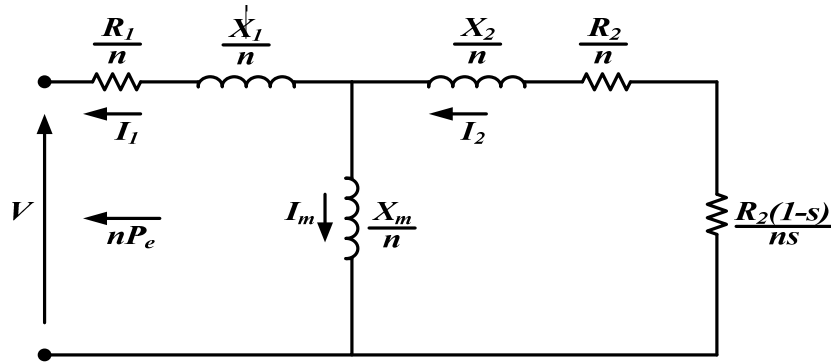


Fig 2.6: Wind farm aggregate circuit

Fig 2.6 shows the wind farm equivalent circuit after aggregation. The parameter “ $n$ ” denotes the total number of wind turbines within the park. The magnitude of all the circuit components is divided by it, because the turbines are grouped in parallel with an equivalent impedance equals to  $\frac{\overline{Z_{eq}}}{n}$ , and they experience the same wind speed. The active power is modified in the first step of the algorithm to include the cumulative turbine injections  $nP_e$ . This results in the elimination of the fifth step since the solution of the circuit in Fig. 2.6 produces the reactive power consumption of the whole wind farm.

The described algorithm is exact and adequately applies to pitch controlled wind turbines. It has been implemented and its simulation results have been validated with those of reference [31], which uses another method to solve the load flow problem.

## **2.4 Summary**

This chapter demonstrates all the required concepts for wind turbine modeling in power flow studies. It sheds lights on some windmill power flow models in the literature and discusses the implemented algorithm in this research.

## CHAPTER 3

# SYNCHRONOUS MACHINE AND WIND TURBINE MODELING IN TRANSIENT STABILITY STUDIES

Stability is defined as the tendency of a power system to maintain equilibrium after the occurrence of a disturbance in its electromechanical dynamic behavior. A power system tends to return to its normal operating conditions through producing restorative forces, which try to overcome the disturbing forces and hold the machines in synchronism [32]. Stability studies are of two types: steady-state or small signal stability, and transient stability. Small signal stability deals with gradual power changes or small disturbances. If these perturbations last for a long time then steady state stability is termed as dynamic or long term stability. Transient stability refers to the capability of a power system to recover from an abrupt severe disturbance. Its period of study varies from one to ten seconds depending on whether first swing or multi swing stability is being examined. The current chapter investigates the synchronous machine dynamic models for both first and multi swing stability. Emphasis will be more on multi swing stability as it requires a more elaborate component model, which can mimic the machine's response in reality. The transient model of a fixed speed wind turbine is also detailed with its inherent assumptions.

### **3.1 Mechanical Dynamics of a Synchronous Machine**

During steady-state, the relative position of the rotor's magnetic axis (direct axis) with respect to a synchronously rotating reference axis is fixed in space. The angle between the two axes is known as the power angle  $\delta$ . Following any disturbance, the

rotor will accelerate or decelerate under the action of imbalance between the mechanical input torque and the developed electrical torque. Hence, a relative motion between the two axes starts to exist. In what follows, the mechanical equation that governs the rotor's dynamics is developed.

The mechanical equation of a rotor in its dynamic state is derived from Newton's second law, which states that the accelerating torque is equal to the product of the moment of inertia and the angular speed. Thus, the swing equation of a synchronous machine may be written as:

$$J \frac{d^2 \theta_m}{dt^2} = T_m - T_e = T_a \quad (3.1)$$

Where,  $J$  is the moment of inertia of the rotor in  $\text{Kg.m}^2$ , and  $\theta_m$  is its mechanical angular displacement with respect to the armature stationary axis in radians (rd).  $T_m$  and  $T_e$  denote the mechanical and electric torques in Newton-meters (N.m) respectively. Their difference results in the accelerating torque  $T_a$ . The mechanical angular displacement  $\theta_m$  can be expressed in the following form based on Fig 3.1 hereunder:

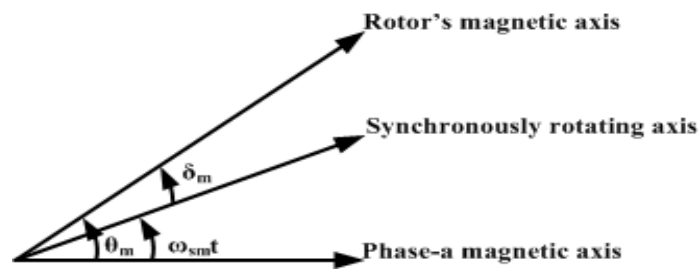


Fig 3.1: Synchronous generator angles in space

$$\theta_m = \omega_{sm} t + \delta_m \quad (3.2)$$

Where,  $\omega_{sm}$  is the synchronous speed in mechanical radians per second (rd/sec),  $t$  is the time in seconds, and  $\delta_m$  is the power angle in mechanical radians (rd). We recall from

this formula that  $\theta_m$  increases continuously with time even during steady-state.

Therefore, it is inconvenient to measure the rotor's displacement from a stationary magnetic axis, since the latter cannot produce any information about the rotor's speed deviation from the synchronous speed. As a result, the angle  $\delta_m$  is introduced to determine the rotor's angular position from a synchronously rotating reference axis, and model the rotor's speed variation from the synchronous speed [32]. The following relations are used to derive the swing equation of a synchronous generator with  $\delta_m$  as the variable of integration.

By taking the first and second derivatives of equation (3.2) we obtain:

$$\omega_m = \frac{d\theta_m}{dt} = \omega_{sm} + \frac{d\delta_m}{dt} \quad (3.3a)$$

$$\frac{d\omega_m}{dt} = \frac{d^2\theta_m}{dt^2} = \frac{d^2\delta_m}{dt^2} \quad (3.3b)$$

Equation (3.3a) shows that the angular speed of the rotor is the sum of the synchronous speed and the instantaneous alteration of  $\delta_m$  with time. During steady state,  $\delta_m$  is constant and the rotor rotates at synchronous speed. If a transient fault occurs, the rotor will accelerate according to the change of  $\delta_m$ . This circumstance justifies the importance of using  $\delta_m$  in inspecting the rotor speed variations. The rotor's acceleration can be calculated from the second derivative of  $\delta_m$  as shown by equation (3.3b). Thus by substituting (3.3b) in (3.1), the swing equation will be written in the following form:

$$J \frac{d^2\delta_m}{dt^2} = T_m - T_e = T_a \quad (3.4)$$

Bearing in mind that power equal torque times angular speed then (3.4) will be given as:

$$J\omega_m \frac{d^2\delta_m}{dt^2} = P_m - P_e = P_a \quad (3.5)$$

The coefficient  $J\omega_m$  is the angular momentum in joule-seconds per mechanical radians. At synchronous speed it is denoted by  $M$  and known as the inertia constant of the machine. However, it is assumed in transient stability studies that the rotor's speed does not vary significantly from the synchronous speed when the machine is stable, thus equation (3.5) becomes:

$$M \frac{d^2\delta_m}{dt^2} = P_m - P_e = P_a, \quad M = J\omega_{sm} \quad (3.6)$$

The quantity  $M$  is not usually supplied with machine data, but rather included within a constant  $H$  that is normally encountered in transient stability problems. The latter is given by

$$H = \frac{\frac{1}{2}J\omega_{sm}^2}{S_{mach}} = \frac{\frac{1}{2}M\omega_{sm}}{S_{mach}} \text{ MJ/MVA} \quad (3.7)$$

in which, the numerator includes the stored kinetic energy of the machine at synchronous speed, and  $S_{mach}$  is the machine's three phase power rating in megavoltamperes. If we solve for  $M$  and replace it in equation (3.6) we get

$$\frac{2H}{\omega_{sm}} \frac{d^2\delta_m}{dt^2} = P_m - P_e = P_a \text{ per unit} \quad (3.8)$$

such that the mechanical and electrical powers are both in per unit on the same base as  $H$ . The synchronous speed and the power angle can be in mechanical or electrical units, but the latter is always preferred. Thus the final form of the swing equation will be :

$$\frac{2H}{\omega_s} \frac{d^2\delta}{dt^2} = P_m - P_e = P_a \text{ per unit} \quad (3.9)$$

As can be seen,  $\omega_s$ , and  $\delta$  have no subscripts, which indicate that they're expressed in electrical units. Equation (3.9) can be divided further into two first order differential equations:

$$\frac{2H}{\omega_s} \frac{d\omega}{dt} = P_m - P_e = P_a \text{ per unit} \quad (3.10)$$

$$\frac{d\delta}{dt} = \omega - \omega_s \quad (3.11)$$

The two variables  $\omega$  and  $\omega_s$  are the rotor and machine synchronous speeds respectively.

They are computed in electrical units and are equivalent to

$$\omega = 2\pi f \quad (3.12a)$$

$$\omega_s = 2\pi f_s \quad (3.12b)$$

with  $f$  being the frequency at rotor's speed and  $f_s$  the frequency at synchronous speed.

The established mechanical model demonstrates the rotor's electromechanical dynamic response and is common to all types of stability studies. The developed electrical power  $P_e$  varies with  $\delta$ , and is computed using the network algebraic equations. The mechanical power is constant throughout the period of study because the action of the speed governor is not modeled in this research. The described model is incorporated in both the first and the multi-swing stability problems regardless of the differences in their electrical characteristics.

### **3.2 Synchronous Machine Electrical Equations**

Synchronous machine models differ in transient stability with the period of simulations. For instance, the classical machine model is implemented in first swing stability that lasts for one second, whereas, the d-q axis machine model is adopted in multi-swing stability that extends up to ten seconds. This section briefly outlines the classical model, and presents a thorough description of the two axis model, which is of our interest in this work.

### 3.2.1 Classical Synchronous Machine Model

The classical machine theory is suitable for transient stability studies that last for a period of one second, i.e. first swing stability. The machine model avoids any differential equations in its electrical circuits, and the flux linkages are considered constant. The equivalent electrical circuit is made up from a transient internal voltage  $\vec{E}'$  that lies behind a transient reactance and an armature resistance. Hence, only one algebraic equation exists, and characterizes the machine's electrical response, i.e.

$$\left| \vec{E}' \right| \angle \delta_i = \vec{V}_i + \vec{I}_i (R_a + jX') \quad (3.13)$$

The initial values of the voltage and current of a unit “*i*” are obtained from the load flow solution prior to disturbance. The magnitude of the transient internal voltage  $\vec{E}'$  remains constant for both cylindrical and salient pole machines, while the power angle  $\delta$  is rectified at every time step in the transient period. The latter is computed from equations (3.10) and (3.11) using one of the commonly used numerical integration techniques. In this work, the implicit trapezoidal method is utilized for its advantages over the others [33-34].

### 3.2.2 Two Axis Synchronous Machine Model

When the simulation time ranges from one to ten seconds, it becomes essential to use more elaborate machine models and include adequate control schemes. In this sense, the d-q axis machine model is favored due to its reasonable precision in demonstrating the generator's dynamic behavior. This model is applicable for round rotor and salient pole machines in the transient state, as the former is a special case of the latter. Though, it is required first to understand the operation of the salient pole machine in the steady state and this is detailed below:



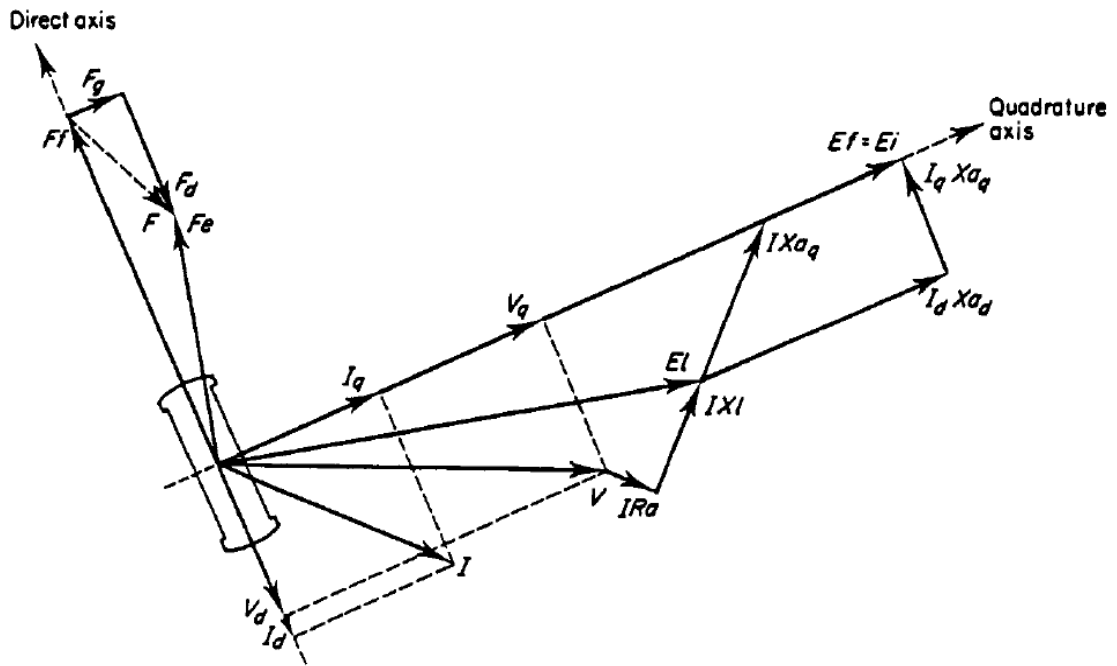


Fig 3.2: Phasor diagram of a salient pole synchronous machine in the steady-state  
Source: [34]

Figure 3.2 portrays the flux and voltage phasor diagram of a salient pole machine in its steady state. In contrast to a cylindrical machine, the armature reaction flux  $F$  is not necessarily in phase with the current  $I$ , nor proportional to it. But instead, its axial components on the direct and quadrature axes are proportional to those of the current as shown in the diagram. The resulting air gap flux  $F_e$  is found by the vectorial addition of the field flux  $F_f$  and the armature reaction flux  $F$ . The terminal voltage  $V$  and the current  $I$  are in the network frame of reference that rotates at synchronous speed. These are interfaced with the machine and transformed to the generator's frame of reference based on the initial position of the rotor's quadrature axis, which is specified by its displacement from the network reference axis. The angle that separates the two axes is the power angle  $\delta$  and it is determined from the following relation:

$$\vec{E}_{qi} = \vec{V} + \vec{I}R_a + \vec{I}(jX_l + jX_{aq}) \quad (3.14a)$$

$$\vec{E}_{qi} = \vec{V} + \vec{I}(R_a + jX_q) \rightarrow \vec{E}_{qi} = |\vec{E}_{qi}| \angle \delta_i \quad (3.14b)$$

$\vec{E}_{qi}$  is a fictitious voltage used for the purpose of locating the machine q-axis. The direct and quadrature synchronous reactances are given by:

$$X_q = X_l + X_{aq} \quad (3.15)$$

$$X_d = X_l + X_{ad} \quad (3.16)$$

The axial components of the voltage are inferred from Fig 3.3 hereunder:

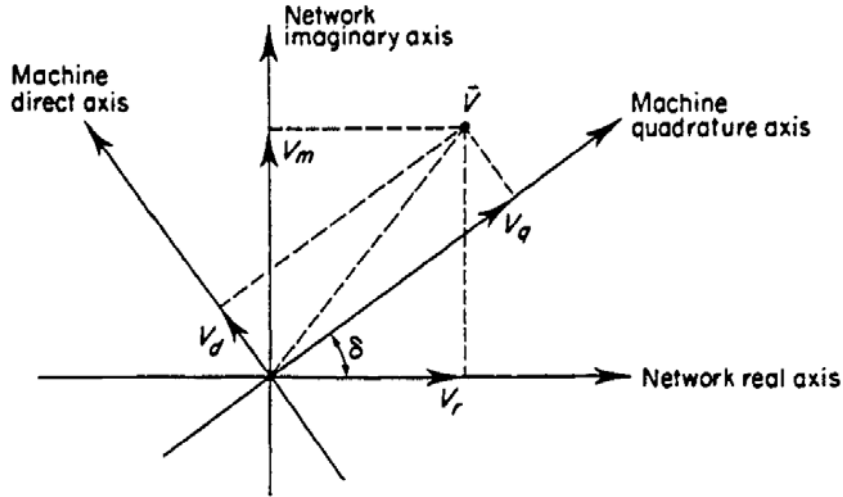


Fig 3.3: Synchronous machine and network frames of reference  
Source: [34]

$$\begin{bmatrix} V_q \\ V_d \end{bmatrix} = \begin{bmatrix} \cos\delta & \sin\delta \\ -\sin\delta & \cos\delta \end{bmatrix} \begin{bmatrix} V_r \\ V_m \end{bmatrix} \quad \text{and} \quad \begin{bmatrix} V_r \\ V_m \end{bmatrix} = \begin{bmatrix} \cos\delta & -\sin\delta \\ \sin\delta & \cos\delta \end{bmatrix} \begin{bmatrix} V_q \\ V_d \end{bmatrix} \quad (3.17)$$

Where,  $V_r$  and  $V_m$  are the real and imaginary components of the voltage in the network frame of reference. These transformations are equally valid for the current. The steady state algebraic equations of the stator that characterize this model are derived by setting all the transient time constants to zero according to [32-34]:

$$E_q = E_i = V_q + I_q R_a - I_d X_d \quad (3.18)$$

$$E_d = 0 \quad (3.19)$$

$$V_d = -I_q X_q - I_d R_a \quad (3.20)$$

$E_i$  denotes the generator's internal voltage and lies completely on the quadrature axis whether in transient or steady state, and  $E_d$  is always equal to zero.

The portrayed diagram in Fig 3.2 is only used to specify the quadrature axis position and initialize the value of the power angle  $\delta$ . Equation (3.13) is also applicable for cylindrical rotor machines since  $X_d \cong X_q$ . However, during a transient state  $E_d$  is not equal to zero because  $E_i$  departs from the q-axis as illustrated in Fig 3.4 below:

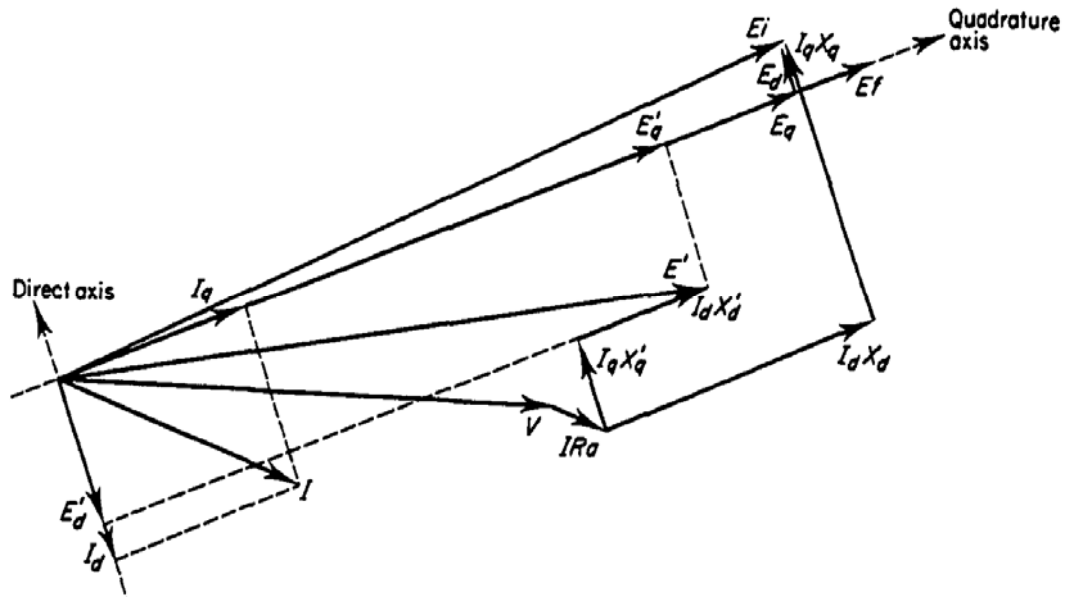


Fig 3.4: Phasor diagram of a synchronous machine in the transient state  
Source: [34]

The phasor diagram in Fig 3.4 corresponds to a round rotor synchronous machine operating in its transient state. In this model, the rotor has one field winding on the direct axis and an equivalent damper winding on the quadrature axis. The transient

voltages  $E'_q$  and  $E'_d$  form the axial quantities of the transient internal voltage  $\vec{E}'$ .  $E'_q$  is affected by the flux linkages of the field winding whereas  $E'_d$  is dependent on the flux linkages of the equivalent winding on the q-axis [33]. Both exist behind the transient reactances  $X'_d$  and  $X'_q$  and are given by [34]:

$$E'_q = V_q + I_q R_a - I_d X'_d \quad (3.21)$$

$$E'_d = V_d + I_d R_a + I_q X'_q \quad (3.22)$$

The rotor flux linkages and hence the corresponding transient voltages are allowed to change according to:

$$\frac{dE'_q}{dt} = \frac{1}{T'_{d0}} [E_f + (X_d - X'_d)I_d - E'_q] \quad (3.23)$$

$$\frac{dE'_d}{dt} = \frac{1}{T'_{q0}} [-(X_q - X'_q)I_q - E'_d] \quad (3.24)$$

where,  $T'_{d0}$  and  $T'_{q0}$  are the transient time constants in seconds. If a salient pole machine is considered then equations (3.22) and (3.24) will be omitted since  $E'_d$  is zero and  $X_q$  is equal to  $X'_q$ .

The machine can still be modeled in its transient state by its Thevenin or Norton equivalent, which when projected on the direct and quadrature axis must yield equations (3.21) and (3.22). The corresponding transient circuit model is as follows:

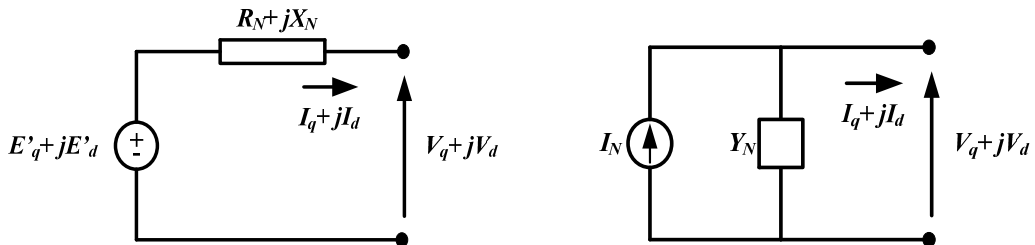


Fig 3.5: Machine transient equivalent circuits

It is obtained by multiplying equation (3.22) by the complex number “j” and adding it to equation (3.21):

$$E'_q + jE'_d - (V_q + jV_d) = R_a(I_q + jI_d) - I_d X'_d + jI_q X'_q \quad (3.25a)$$

$$E'_q + jE'_d - (V_q + jV_d) = (I_q + jI_d) \left[ R_a - \frac{I_d X'_d}{I_q + jI_d} + \frac{jI_q X'_q}{I_q + jI_d} \right] \quad (3.25b)$$

$$E'_q + jE'_d - (V_q + jV_d) = (I_q + jI_d) \left[ R_a + \frac{I_q I_d (X'_q - X'_d)}{I_q^2 + I_d^2} + j \frac{I_d^2 X'_d + I_q^2 X'_q}{I_q^2 + I_d^2} \right] \quad (3.25c)$$

Thus, the generator's impedance and the Norton current can be found correspondingly from equation (3.25c) as

$$R_N = R_a + \frac{I_q I_d (X'_q - X'_d)}{I_q^2 + I_d^2} \quad (3.26)$$

$$X_N = \frac{I_d^2 X'_d + I_q^2 X'_q}{I_q^2 + I_d^2} \quad (3.27)$$

$$I_N = \frac{E'_q + jE'_d}{R_N + X_N} = (E'_q + jE'_d) Y_N \rightarrow I_{Nq} + jI_{Nd} \quad (3.28)$$

and the air gap power in per-unit is equal to:

$$P_e = E'_q I_q + E'_d I_d \quad (3.29)$$

It is clear that the Norton admittance is a function of the terminal current components and hence depends on  $\delta$ , which in turn is time dependent. It should be noted that the network is modeled by its nodal admittance matrix  $[Y]$  and all loads are converted to shunt admittances  $y_{di}$ :

$$[I_{inj}] = [Y][V] \quad (3.30)$$

$$y_{di} = \frac{P_{di} - jQ_{di}}{|V_i|^2} \quad (3.31)$$

The generator and load admittances are usually included in the network admittance matrix  $[Y]$ , which stays constant throughout the simulation period. However, in this

model  $[Y]$  will vary due to the change of the generator's Norton admittance  $Y_N$ , which is modified at each integration step with the terminal current. Hence, it becomes computationally cumbersome to use the proposed circuit model. Alternatively, an adjusted Norton equivalent can be used [34] that retains the accuracy of the machine's Norton circuit while keeping the network bus admittance matrix always constant. This is achieved by manipulating the machine's Norton equivalent into the following circuit:

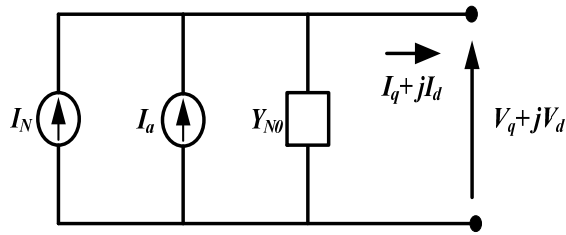


Fig 3.6: Adjusted Norton equivalent circuit

The generator's admittance is replaced by  $Y_{N0}$ , whose value is estimated to [34]:

$$Y_{N0} = \frac{R_a - j \frac{X'_d + X'_q}{2}}{R_a^2 + X'_d X'_q} \quad (3.32)$$

The terminal current is identical in the exact and the adjusted Norton circuits such that:

$$I_N - Y_N V = I \quad (3.33a)$$

$$I_N + I_a - Y_{N0} V = I \quad (3.33b)$$

By equating (3.32a) and (3.32b),  $I_a$  will be determined as:

$$I_a = (Y_{N0} - Y_N) V \quad (3.34)$$

The proposed transient model is combined with the mechanical model to produce a 4<sup>th</sup> order integration model for the synchronous machine. In what follows, the generator's excitation system model will be discussed.

### 3.3 Automatic Voltage Regulator

The primary function of an automatic voltage regulator is to maintain a constant voltage level at the terminals of a generator. Several excitation system models have been defined by the IEEE to represent the control action, which takes place within a synchronous machine. The main two are the Type 1 and Type 2 systems [34]. In this research, the Type 1 system is employed and it is described below:

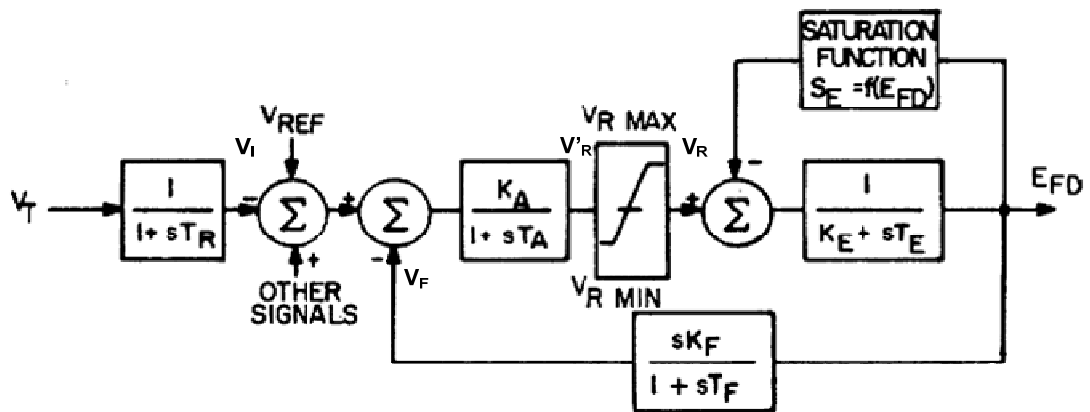


Fig 3.7: IEEE Type 1 excitation system model  
Source: [35]

The parameters of the shown block diagram are as follows:

- $V_T$  is the generator's terminal voltage.
- $T_R$  is the time constant of the input filter in seconds.
- $V_i$  is the filter's output voltage.
- $V_{REF}$  is the reference voltage signal. It is usually calculated with the initialization procedure of the regulator variables.
- $K_A$  is the amplifier gain.
- $T_A$  is the amplifier time constant in seconds

- $V'_R$  is the amplifier output voltage.
- $V_{R\ MIN}$  and  $V_{R\ MAX}$  are the amplifier lower and upper limits.
- $V_R$  is the limiter output voltage.
- $K_E$  is the exciter gain.
- $T_E$  is the exciter time constant in seconds.
- $E_{FD}$  is the field voltage and is equal to  $E_f$  in figures 3.2 and 3.3.
- $S_E$  is the saturation function of the field voltage.
- $K_F$  is the stabilizer gain.
- $T_F$  is the stabilizer time constant in seconds.
- $V_F$  is the stabilizer output voltage.

The dynamic equations for the current model are derived from the given transfer function. These comprise those of the input filter, the amplifier, the exciter and the stabilizer. The input filter differential equation is given by

$$\frac{dV_I}{dt} = \frac{1}{T_R} [V_T - V_I] \quad (3.35)$$

and that of the amplifier is

$$\frac{dV'_R}{dt} = \frac{1}{T_A} [K_A(V_{REF} - V_I - V_F) - V'_R] \quad (3.36)$$

Equation (3.35) is subject to the following constraint

$$V_{R\ MIN} \leq V'_R \leq V_{R\ MAX} \quad (3.37)$$

where

$$V_R = V_{R\ MIN} \text{ if } V'_R < V_{R\ MIN}$$

or

$$V_R = V_{R\ MAX} \text{ if } V'_R > V_{R\ MAX}$$

$$\text{else } V_R = V'_R$$



The excitation voltage varies according to

$$\frac{dE_{FD}}{dt} = \frac{1}{T_E} [V_R - (S_E + K_E)E_{FD}] \quad (3.38)$$

and the operation of the stabilizer in the feedback loop is governed by:

$$\frac{dV_F}{dt} = \frac{1}{T_F} \left\{ \frac{K_E}{T_E} [V_R - (S_E + K_E)E_{FD}] - V_F \right\} \quad (3.39)$$

The expression of the saturation function  $S_E$  has been highlighted in reference [34]. The latter states that the “IEEE recommends that  $S_E$  be specified at maximum field voltage ( $S_{E \max}$ ) and at 0.75 of maximum field voltage ( $S_{E 0.75 \max}$ ). From this  $S_E$  may be determined for any value of field voltage by either linear interpolation or by fitting a quadratic function”. Hence, if linear interpolation is selected, the graphical representation of  $S_E$  versus  $E_{FD}$  will be divided into two linear regions such that

$$S_E = K_1 E_{FD} - K_2 \quad (3.40)$$

in which

$$K_1 = \frac{4S_{E 0.75 \max}}{3E_{FD \max}}, K_2 = 0 \text{ if } E_{FD} \leq E_{FD 0.75 \max} \quad (3.41)$$

or

$$K_1 = \frac{4(S_{E \max} - S_{E 0.75 \max})}{E_{FD \max}}, K_2 = 4S_{E 0.75 \max} - 3S_{E \max} \text{ if } E_{FD} \geq E_{FD 0.75 \max} \quad (3.42)$$

The described excitation system is merged with the two-axis machine model to result in an 8<sup>th</sup> order model for the generator. All the mentioned variables are expressed in per-unit notation. The time constants, the angular speeds, and the power angle are kept in their respective units. The initialization procedure of this model will be explained in the last part of the chapter. The next section presents the transient machine model of a fixed speed wind turbine.

### 3.4 Wind Turbine Dynamic Modeling

Wind turbine modeling in transient stability studies has been examined explicitly. Different drive train models have been tested in an attempt to identify the most accurate model, which practically demonstrates the windmill dynamic behavior during a fault period. The electrical subsystem has been also explored extensively through inspecting three generator types and noting their global influence on the stability of a power system. Though, consideration in this work is only given to squirrel cage induction generators (SCIG's) as they are installed in fixed speed wind turbines. This division of the chapter establishes the employed windmill transient model. An analogous approach to that adopted in modeling a synchronous machine is used.

#### 3.4.1 Mechanical Model of a Wind Turbine

The mechanical model of a windmill is divided into two major parts that include the rotor model and the shaft model:

##### 3.4.1.1 The rotor model

The extracted mechanical power by a wind turbine is calculated from the following relation:

$$P_m = \frac{1}{2} \rho A_R v^3 C_p(\lambda, \theta) \quad (2.1)$$

Using the above equation, the mechanical torque can be equated as:

$$T_m = \frac{P_m}{\omega_r} = \frac{\frac{1}{2} \rho A_R v^3 C_p(\lambda, \theta)}{\omega_r} \quad (3.43)$$

By introducing the formula of the tip speed ratio (Eq. 2.2) in (3.43), the torque will be written as:

$$T_m = \frac{1}{2} \rho A_R v^2 \frac{C_p(\lambda, \theta) R}{\lambda} = \frac{1}{2} \rho A_R v^2 C_t(\lambda, \theta) R \quad (3.43)$$

Where,  $C_t$  is known as the torque coefficient, and has a similar plot to the  $(C_p, \lambda)$  curve. Thus, at a given pitch angle  $C_t$  will vary due to the change of either the wind velocity or the angular speed. In this thesis, the operation of the pitch controller during the transient period is not modeled. Hence, the torque coefficient will only be dependent on  $\lambda$ . It has been stated in the literature that when transient stability is being investigated under the case of a fault, the wind velocity may be considered constant provided that the time span does not exceed 10 seconds [9, 13, 17, and 21]. Knowing this, the torque coefficient may be only expressed in terms of the angular speed  $\omega_r$ , and the mechanical torque will change along with the latter. However, references [4-8] and [13] suggest that the torque may be assumed constant since the angular speed varies within a narrow range in a SCIG. Therefore, it is kept constant throughout the simulation period. Its magnitude is initially calculated from the generator's developed torque in view of the fact that both quantities are equal during steady state.

#### 3.4.1.2 The shaft model

The equation of motion of a wind turbine relies on the shaft model representation. The most two recognized models are the one mass and the two mass models. In the former, all the components of the turbine are lumped into one mass, whereas in a two mass model the generator and turbine rotors are two separate masses that swing with respect to each other. The shaft that connects them is normally chosen to be the one with low speed. This is due to the fact that the resonance frequencies of the gearbox and high speed shaft are much higher than that of the low speed shaft, which is normally 2Hz and lies in the range of interest 0.1-10 Hz [36].

The rotating mass in a one mass model exhibits the following dynamics:

$$J_t \frac{d\omega_g}{dt} = T_m - T_e \quad (3.44)$$

Where,  $J_t$  is the total moment of inertia of all the rotating masses, and  $\omega_g$  is the angular speed of the generator. Solving for  $J_t$  in (3.7) and substituting it in (3.44) yields:

$$\frac{2HS_{mach}}{\omega_{sm}^2} \frac{d\omega_g}{dt} = T_m - T_e \quad (3.45)$$

Dividing equation (3.45) by  $T_{base} = S_{base}/\omega_{base} = S_{mach}/\omega_{sm}$  gives:

$$\frac{2H}{\omega_{sm}} \frac{d\omega_g}{dt} = \frac{T_m - T_e}{T_{base}} \quad (3.46)$$

The generator's developed torque  $T_e$  is given by:

$$T_e = \frac{P_g}{\omega_{sm}} \quad (3.47)$$

$P_g$  is the air gap power in an induction machine, and  $\omega_{sm}$  is obtained from

$$\omega_{sm} = \frac{2}{p} \omega_s = \frac{2}{p} 2\pi f \quad (3.48)$$

where  $p$  is the number of poles. Knowing that the slip is

$$s = \frac{\omega_{sm} - \omega_g}{\omega_{sm}} \quad (3.49)$$

its first derivative will be:

$$\frac{ds}{dt} = -\frac{1}{\omega_{sm}} \frac{d\omega_g}{dt} \quad (3.50)$$

Introducing equation (3.50) in (3.46) produces:

$$2H \frac{ds}{dt} = T_e - T_m \text{ per unit} \quad (3.51)$$

Equation (3.51) characterizes the mechanical dynamics of a one mass model. The shaft stiffness is infinite on the contrary to a two mass model which is illustrated in Fig 3.8:

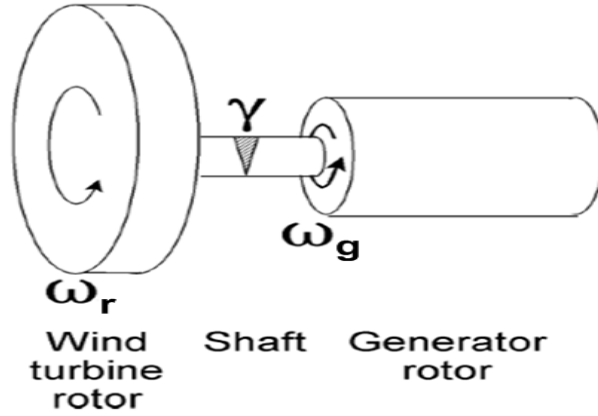


Fig. 3.8 Two mass model representation  
Source: [36]

The dynamic equations of this model are:

$$\frac{2H_r}{\omega_{sm}} \frac{d\omega_r}{dt} = \frac{T_m - K_s\gamma}{T_{base}} \rightarrow 2H_r \frac{d\omega_r}{dt} = T_m - K_s\gamma \text{ per unit} \quad (3.52)$$

$$\frac{2H_g}{\omega_{sm}} \frac{d\omega_g}{dt} = \frac{K_s\gamma - T_e}{T_{base}} \rightarrow 2H_g \frac{d\omega_g}{dt} = K_s\gamma - T_e \text{ per unit} \quad (3.53)$$

$$\frac{d\gamma}{dt} = \omega_{sm}(\omega_r - \omega_g) \quad (3.54)$$

Where,  $\gamma$  is the torsional twist angle between the turbine's end and the generator's end in mechanical radians, and  $K_s$  is the shaft stiffness in p.u torque per mechanical radians.  $\omega_r$  and  $\omega_g$  are the angular speeds of the turbine and generator respectively. They are expressed in per unit with  $\omega_{sm}$  as the angular speed base. The turbine and generator inertia constants are denoted by  $H_r$  and  $H_g$ . If a wind farm is modeled, then the total inertia constant and shaft stiffness of the equivalent windmill will be the sum of the individual inertia and stiffness constants. This assumption is valid when the turbines have the same natural torsional frequency and the wind speed is identical across the entire farm [3].

### 3.4.2 Induction Machine Transient Model

The transient circuit of an induction machine can be modeled in the same manner as the synchronous machine using the Thevenin or Norton equivalents. Thus, the machine may be represented by a transient internal voltage  $\vec{E}'$ , which lies behind a transient reactance and an internal resistance as depicted below:

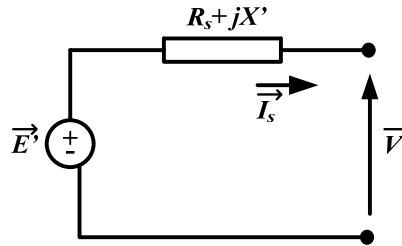


Fig 3.9: Induction generator circuit in the transient state

The resistance  $R_s$  is the stator's resistance and the reactance  $X'$  is obtained from the locked rotor test while it is given by

$$X' = X_s + \frac{X_m X_r}{X_m + X_r} \quad (3.55)$$

where  $X_s$  and  $X_r$  are the stator and rotor reactances respectively, and  $X_m$  is the machine magnetizing reactance. The transient internal voltage  $\vec{E}'$  is variable and its rate of change given by [34] is

$$\frac{d\vec{E}'}{dt} = -j2\pi f s \vec{E}' - \frac{1}{T'_0} [(\vec{E}' + j(X_0 - X')\vec{I}_s)] \quad (3.56)$$

in which  $s$  is the slip,  $X_0$  and  $T'_0$  are the open circuit reactance and time constant denoted by:

$$X_0 = X_s + X_m \quad (3.57)$$

$$T'_0 = \frac{X_r + X_m}{2\pi f R_r} \quad (3.58)$$

Knowing that the induction machine reactances are independent of the rotor's position, the entire model can be described in the network frame of reference. Thus,

$$\vec{E}' = E'_r + jE'_m \quad (3.59)$$

$$\vec{I}_s = I_r + jI_m \quad (3.60)$$

where the subscripts  $r$  and  $m$  denote the real and imaginary network axial components.

The per unit value of the generator's air gap power may be given by

$$P_g = E'_r I_r + E'_m I_m \quad (3.61)$$

and the developed torque is equivalent to it when both are expressed in per unit with  $\omega_{sm}$  as the angular speed base. Hence:

$$T_e = E'_r I_r + E'_m I_m \quad (3.62)$$

Equation (3.56) can be projected on the real and imaginary axes to yield:

$$\frac{dE'_r}{dt} = 2\pi f s E'_m - \frac{1}{T'_0} [(E'_r - (X_0 - X')I_m)] \quad (3.63)$$

$$\frac{dE'_m}{dt} = -2\pi f s E'_r - \frac{1}{T'_0} [(E'_m + (X_0 - X')I_r)] \quad (3.64)$$

The two equations above demonstrate the electrical behavior of an induction generator during its transient state. The stator transients are neglected since they are much faster than those of the rotor. Their effect is negligible when the induction machine is a part of a large system. If a wind park is connected, then  $\frac{X'}{n}$ ,  $\frac{X_0}{n}$ , and  $\frac{R_s}{n}$  replace  $X'$ ,  $X_0$ , and  $R_s$  while the time constant  $T'_0$ , and the slip are unaffected.

The current section concludes all the machine models that are implemented in the transient stability problem in this work. In what follows, the complete structure of the transient stability program is detailed.

### 3.5 Structure of a Transient Stability Program

The structure of a transient stability program [34] is as follows:

- Read in the load flow data.
- Read in the transient stability data.
- Read in the switching data.
- Model the loads as constant admittances.
- Initialize the synchronous machine variables.
- Initialize the excitation system variables.
- Initialize the wind turbine variables.
- Print out initialization results.
- Form the network admittance matrix  $Y$  by including:
  - ✓ Network branches
  - ✓ Load admittances
  - ✓ Synchronous generator admittances
  - ✓ Induction generator admittances
- Calculate the bus impedance matrix  $Z_{bus}$  by inverting  $Y$ .
- Set time to zero.
- While time < steady state time:
  - ✓ Check for switching.
  - ✓ Adjust time step if required or keep it at its input value.
  - ✓ Solve for the next time step,  $(m + 1)$  just before switching:
    - for  $r = 1$ : number of iterations
    - Solve the synchronous machine dynamic equations.
    - Solve the excitation system dynamic equations.



- Solve the wind turbine dynamic equations.
  - Calculate the synchronous and induction machine Norton currents.
  - Solve the network equations using  $V_{bus} = Z_{bus}I_{inj}$ .
  - Update the terminal voltages, the machine currents, the accelerating power and the accelerating torque.
  - Check for the convergence of the implicit trapezoidal method.
  - End for loop.
- ✓ Print out the numerical integration results.
- ✓ If there is switching:
- Carry out switching operation.
  - Form the  $Y$  matrix considering switching.
  - Calculate the modified bus impedance matrix  $Z_{bus}$ .
  - Solve the network equations using  $V_{bus} = Z_{bus}I_{inj}$ .
  - Update the terminal voltages, the machine currents, the accelerating power, and the accelerating torque.
  - Print out the results.
- ✓ End if condition.
- End while loop, End algorithm.

The procedure above provides an overview on the organization of a transient stability program with its major parts. The program is split into several sub routines that include the synchronous machine, the excitation system, and the wind turbine models.

## 3.6 Initialization Scheme and the Implicit Trapezoidal Method

The initialization procedure of all the component models is described in this section along with the steps that make up the implicit trapezoidal method.

### 3.6.1 Initial Conditions:

#### 3.6.1.1 Synchronous machine initial conditions

- Calculate the terminal voltage  $V$  and current  $I$  from the load flow solution.
- Locate the machine's quadrature axis from equation (3.14b).
- Transform  $V$  and  $I$  to the machine frame of reference using (3.17a).
- Calculate  $E'_q$ , and  $E'_d$  using (3.21, 3.22).
- Calculate the field voltage  $E_f$  by setting (3.23) to zero
- Calculate the electrical and mechanical powers from (3.29).
- Set the accelerating power  $P_a$  to zero.

#### 3.6.1.2 AVR initial conditions

- Determine the filter's output voltage as  $V_I = V_T$  by setting (3.35) to zero.
- Calculate  $S_e$  from (3.40) using (3.41) or (3.42).
- Calculate  $V_R$  by setting (3.38) to zero. Let  $V'_R = V_R$ . This assumption is valid since:  $V_{R\ MAX} = (S_{E\ max} + K_E)E_{F\ max}$ , which implies that the initial value of the regulator output voltage  $V'_R$  satisfies the constraint in (3.37) as the initial values of  $S_e$  and  $E_F$  are definitely less than maximum.
- Calculate  $V_{REF}$  by setting (3.36) to zero.
- Calculate  $V_F$  by setting (3.39) to zero, thus  $V_F = 0$ .

### 3.6.1.3 Wind turbine initial conditions

- Calculate the terminal voltage  $V$  and current  $I$  from the load flow solution.
- Calculate  $E'_q$ , and  $E'_d$  using (3.63, 3.64).
- Calculate the electrical and mechanical torques from (3.62).
- Calculate  $\theta_s$  by setting (3.52) to zero.
- Setting (3.54) to zero gives  $\omega_r = \omega_g$ .

### **3.6.2 The implicit trapezoidal method:**

- Calculate the initial estimates:
  - ✓  $P_a^0(m+1) = P_a(m)$
  - ✓  $\omega^0(m+1) = \omega(m)$
  - ✓  $E'_q{}^0(m+1) = E'_q(m)$
  - ✓  $E'_d{}^0(m+1) = E'_d(m)$
  - ✓  $I_q{}^0(m+1) = I_q(m)$
  - ✓  $I_d{}^0(m+1) = I_d(m)$
  - ✓  $E_f{}^0(m+1) = E_f(m)$
  - ✓  $V_I{}^0(m+1) = V_I(m)$
  - ✓  $V_T{}^0(m+1) = V_T(m)$
  - ✓  $V'_R{}^0(m+1) = V'_R(m)$
  - ✓  $S_e{}^0(m+1) = S_e(m)$
  - ✓  $E_r{}^0(m+1) = E_r(m)$
  - ✓  $E_m{}^0(m+1) = E_m(m)$
  - ✓  $I_r{}^0(m+1) = I_r(m)$

$$\checkmark I_m^0(m+1) = I_m(m)$$

$$\checkmark \theta^0(m+1) = \theta(m)$$

$$\checkmark T_e^0(m+1) = T_e(m)$$

➤ for  $r = 1$ : number of iterations

$$\checkmark \omega^r(m+1) = \omega(m) + \frac{h}{2M} [P_a(m) + P_a^{r-1}(m+1)]$$

$$\checkmark \delta^r(m+1) = \delta(m) + \frac{h}{2} [\omega(m) + \omega^r(m+1) - 2\omega_s]$$

$$\checkmark E'_q{}^r(m+1) = E'_q(m) + \frac{h}{2T'_{d0}} [E_f(m) + (X_d - X'_d)I_d(m) - E'_q(m) + E_f^{r-1}(m+1) + (X_d - X'_d)I_d^{r-1}(m+1) - E'_q{}^{r-1}(m+1)]$$

$$\checkmark E'_d{}^r(m+1) = E'_d(m) + \frac{h}{2T'_{q0}} [-(X_q - X'_q)I_q(m) - E'_d(m) - (X_q - X'_q)I_q^{r-1}(m+1) - E'_d{}^{r-1}(m+1)]$$

$$\checkmark V_I{}^r(m+1) = V_I(m) + \frac{h}{2T_R} [V_T(m) - V_I(m) + V_T^{r-1}(m+1) - V_I^{r-1}(m+1)]$$

$$\checkmark V'_R{}^r(m+1) = V'_R(m) + \frac{h}{2T_A} [K_A(V_{REF} - V_I(m) - V_F(m)) - V'_R(m) + K_A(V_{REF} - V_I^r(m+1) - V_F^{r-1}(m+1)) - V'_R{}^{r-1}(m+1)]$$

$$\checkmark \text{Check the constraint in (3.37) and compute } V_R{}^r(m+1)$$

$$\checkmark E_f{}^r(m+1) = E_f(m) + \frac{h}{2T_E} [V_R{}^r(m) - (S_e(m) + K_E)E_f(m) + V_R{}^r(m+1) - (S_e^{r-1}(m+1) + K_E)E_f^{r-1}(m+1)]$$

$$\checkmark \text{Calculate } (S_e{}^r(m+1) \text{ using } E_f{}^r(m+1)$$

- ✓  $V_f^r(m+1) = V_f(m) + \frac{h}{2T_F} \left[ \frac{K_F}{T_E} [V_R^r(m) - (S_e(m) + K_E)E_f(m) + V_R^r(m+1) - (S_e^{r-1}(m+1) + K_E)E_f^{r-1}(m+1)] - V_f(m) - V_f^{r-1}(m+1) \right]$
- ✓  $\omega_r^r(m+1) = \omega_r(m) + \frac{h}{4H_r} [T_m(m) - K\theta(m) + T_m(m+1) - K\theta^{r-1}(m+1)]$
- ✓  $\omega_g^r(m+1) = \omega_g(m) + \frac{h}{4H_g} [K\theta(m) - T_e(m) + K\theta^{r-1}(m+1) - T_e^{r-1}(m+1)]$
- ✓  $\theta^r(m+1) = \theta(m) + \frac{h\omega_{sm}}{2} [\omega_r(m) - \omega_g(m) + \omega_r^r(m+1) - \omega_g^r(m+1)]$
- ✓ Calculate the slip  $s^r(m+1)$  from (3.49) using  $\omega_g^r(m+1)$
- ✓  $E'_r{}^r(m+1) = E'_r(m) + \frac{h}{2} \left[ 2\pi f s(m) E'_m(m) - \frac{1}{T'_0} [E'_r(m) - (X_0 - X')I_m(m)] + 2\pi f s^r(m+1) E'_m{}^{r-1}(m+1) - \frac{1}{T'_0} [E'_r{}^{r-1}(m+1) - (X_0 - X')I_m{}^{r-1}(m+1)] \right]$
- ✓  $E'_m{}^r(m+1) = E'_m(m) + \frac{h}{2} \left[ -2\pi f s(m) E'_r(m) - \frac{1}{T'_0} [E'_m(m) + (X_0 - X')I_r(m)] - 2\pi f s^r(m+1) E'_r{}^{r-1}(m+1) - \frac{1}{T'_0} [E'_m{}^{r-1}(m+1) + (X_0 - X')I_r{}^{r-1}(m+1)] \right]$
- ✓ Find the synchronous machine Norton current using  $E'_q{}^r(m+1)$ , and  $E'_d{}^r(m+1)$ , and  $Y_N$ .
- ✓ Calculate the adjustment current  $I_a$ .
- ✓ Calculate the synchronous machine terminal current  $I$ .

- ✓ Transform  $I$  into the network frame of reference using  $\delta^r(m+1)$
- ✓ Find the windmill Norton current using  $E'_{r^r}(m+1)$ , and  $E'_{m^r}(m+1)$ , and the induction machine admittance.
- ✓ Solve the network equations using  $V_{bus} = Z_{bus}I_{inj}$ .
- ✓ Transform the voltages at the synchronous generator nodes to the machine frame of reference.

- ✓ Calculate the synchronous machine terminal current from:

$$\begin{bmatrix} I_q^r(m+1) \\ I_d^r(m+1) \end{bmatrix} = \frac{1}{R_a^2 + X'_d X'_q} \begin{bmatrix} R_a & X'_d \\ -X'_q & R_a \end{bmatrix} \begin{bmatrix} E'_q - V_q \\ E'_d - V_d \end{bmatrix} \quad (3.65)$$

- ✓ Calculate the accelerating power  $P_a^r(m+1)$  as:

$$P_m - [E'_q{}^r(m+1)I_q^r(m+1) + E'_d{}^r(m+1)I_d^r(m+1)] \quad (3.66)$$

- ✓ Calculate the synchronous machine active and reactive power from:

$$P = V_q^r(m+1)I_q^r(m+1) + V_d^r(m+1)I_d^r(m+1) \quad (3.67)$$

$$Q = V_d^r(m+1)I_q^r(m+1) - V_q^r(m+1)I_d^r(m+1) \quad (3.68)$$

- ✓ Calculate the wind turbine terminal current from:

$$\begin{bmatrix} I_r^r(n+1) \\ I_m^r(n+1) \end{bmatrix} = \frac{1}{R_s^2 + X'X'} \begin{bmatrix} R_s & X' \\ -X' & R_s \end{bmatrix} \begin{bmatrix} E'_r - V_r \\ E'_m - V_m \end{bmatrix} \quad (3.69)$$

- ✓ Calculate the wind turbine electric torque,  $T_e^r(m+1)$  as:

$$[E'_r{}^r(m+1)I_r^r(m+1) + E'_m{}^r(m+1)I_m^r(m+1)] \quad (3.70)$$

- ✓ Calculate the windmill active and reactive power using (3.67).

- ✓ Check for convergence. If it is reached, break and end the loop.

➤ End algorithm

The proposed algorithm is sufficient for transient stability studies. It has been used to carry out all the simulations, which will be presented in the subsequent chapter.

### **3.7 Summary**

The component models described in this chapter constitute the building block for dynamic studies. The explained stability program is suitable for transient fault simulations. The program itself can be easily manipulated to include other component models such as those related to machine saturation effects and the speed governing action.

## CHAPTER 4

### WINDMILL MODEL VALIDATION RESULTS AND A CASE STUDY ON THE LEBANESE POWER SYSTEM

Power flow analysis with grid-connected wind turbines along with machine modeling in transient stability studies have been explored thoroughly throughout this thesis. The current chapter introduces the windmill model validation results, which has been obtained using the described load flow and transient stability programs. Both are written in MATLAB and used to carry out a case study on the 220/150 KV Lebanese network with an integrated wind park. A three phase fault is applied in the vicinity of the wind farm to assess its dynamic behavior and study the effect of several parameters, such as the reactive power compensation, the fault location, and the penetration levels on the critical clearing time.

#### **4.1. Wind Turbine Model Validation Results**

In order to emphasize the validity of the proposed load flow and transient stability algorithms, a single machine infinite bus system is tested. This consists of a wind turbine that connects to an infinite bus through a Thevenin equivalent impedance or a transmission line. It is usually employed for its simplicity and capability to illustrate the steady state and dynamic response of a windmill. Hence, all the qualitatively discussed ideas in the literature could be noted and proved in a quantitative manner. This section includes the load flow and transient stability simulation results of the wind turbine infinite bus system.



#### 4.1.1 Wind Turbine Load Flow Results

The test system of reference [31] is used to validate the suggested power flow algorithm. The network is modeled by a Thevenin equivalent impedance that is equal to  $0.01 + j0.1$  p.u on a 100 MVA base, and the asynchronous machine data is that of Table 2.1. The load flow problem is solved for different input values of the electrical output power  $P_e$ , which correspond to various wind speeds. The machine's operational parameters including the terminal voltage  $V$ , the consumed reactive power  $Q_e$ , and the slip  $S$ , are noted and their values in p.u are given by the following table:

Table 4.1: The Proposed PQ Model Load Flow Results

$P_e$ (Generated)	$V$	$Q_e$ (Consumed)	$S$
0.5941	0.9592	0.4298	-0.0043
0.6921	0.9553	0.4676	-0.0051
0.7897	0.9504	0.5130	-0.0059
0.8868	0.9443	0.5674	-0.0068
0.9833	0.9367	0.6329	-0.0079
1.0789	0.9270	0.7132	-0.0091

It is obvious from the table above that an increase in wind power triggers a further drop in voltage at the machine terminals, as a result of the increased consumption of reactive power. The latter is nearly proportional to the slip, which in turn acquires higher values when the active power generation rises as displayed in the figure hereunder:

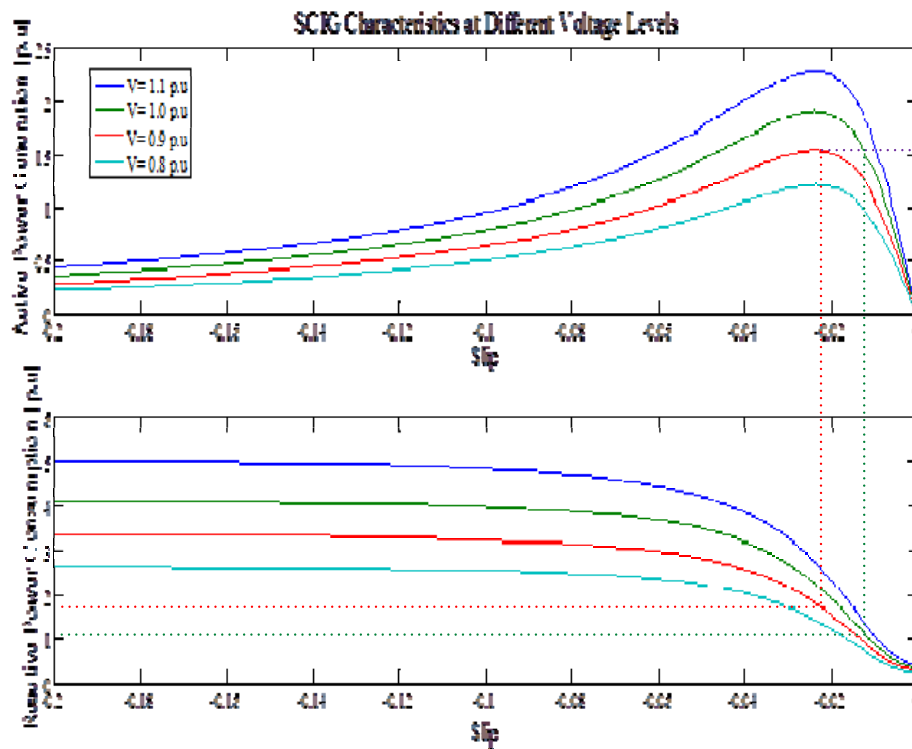


Fig 4.1: Active power generation and reactive power consumption at the terminals of a SCIG as a function of the slip and voltage

Figure 4.1 shows the active and reactive power variation in a SCIG as a function of the slip and the terminal voltage [36]. At a given terminal voltage the active and reactive powers change proportionally with the slip. This is true as long as the maximum power point is not exceeded. The green and red dotted lines, which correspond to 1.0 and 0.9 p.u. terminal voltages respectively, support the earlier results of Table 4.1. For instance, at a lower terminal voltage, the machine consumes more reactive power and spins at a higher speed. This circumstance is only encountered when the active power generation at the lower voltage requires a much larger slip than that at the higher voltage. Since the reactive power demand of the red line will only surpass the green one in case the difference in slip is notable.

#### 4.1.2 Wind Turbine Transient Stability Results

The system under consideration in this study is that of reference [7]. It is formed by a wind turbine that connected to an infinite bus through a step-up transformer and a double circuit transmission line. Its relevant data is detailed in the following table:

Table 4.2: Wind turbine infinite bus system data

Source: [7]

Main parameters	Value
Rated power $P_N$ (MW)	3
Rated voltage $U_N$ (V)	575
Rated frequency $f_N$ (Hz)	60
Stator resistance $R_s$ (p.u.)	0.004843
Rotor resistance $R_r$ (p.u.)	0.004347
Stator leakage inductance $X_{s\sigma}$ (p.u.)	0.1248
Rotor leakage inductance $X_{r\sigma}$ (p.u.)	0.1791
Mutual inductance $X_m$ (p.u.)	6.77
Generator rotor inertia constant $H_G$ (s) in per unit	0.5
Wind turbine rotor inertia constant $H\omega$ (s) in per unit	4.54
Shaft stiffness $K_s$ (p.u./el.rad)	0.3
Transformation reactance $X_{tr}$ (p.u.)	0.025
A single transmission line reactance $X_l$ (p.u.)	0.0013

The wind turbine parameters in Table 4.2 are those of a typical 3 MW generating unit. There per unit values are based on the machine's nominal power, while the system reactances are on a 100 MVA base. The transient behavior of the windmill during a symmetrical fault at  $t=2.0$  seconds is examined with both the one and two mass shaft models. The results are portrayed by the figures below:

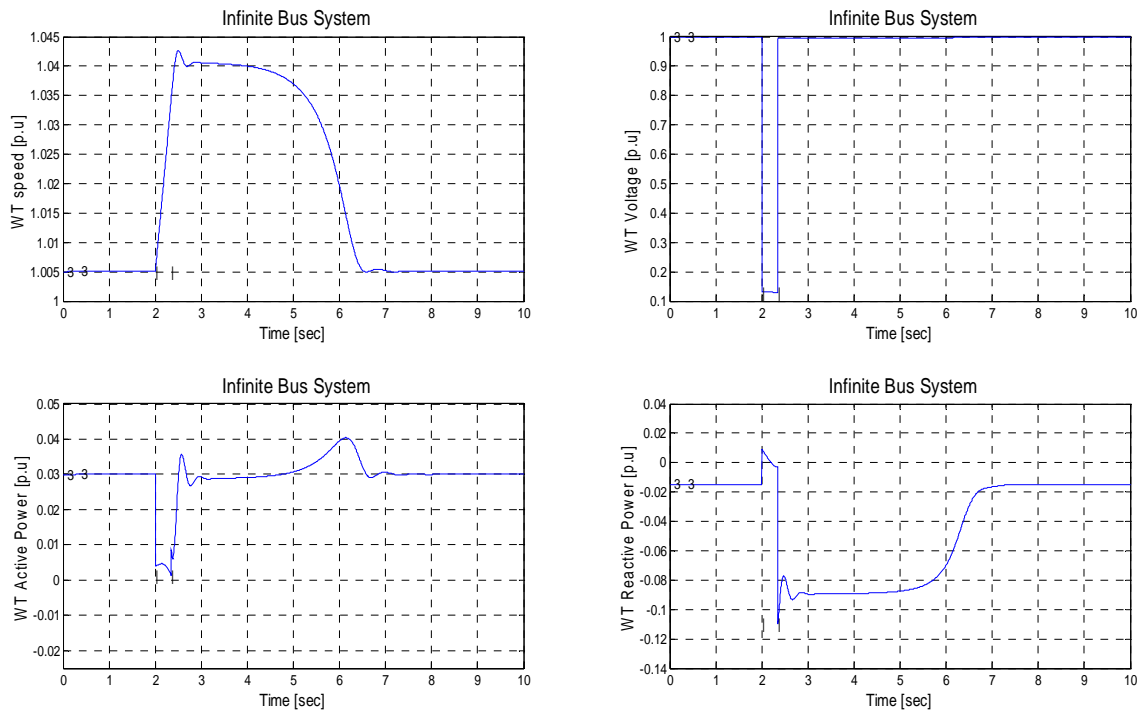


Fig 4.2a: One mass model transient response with a fault clearing time of 349 ms

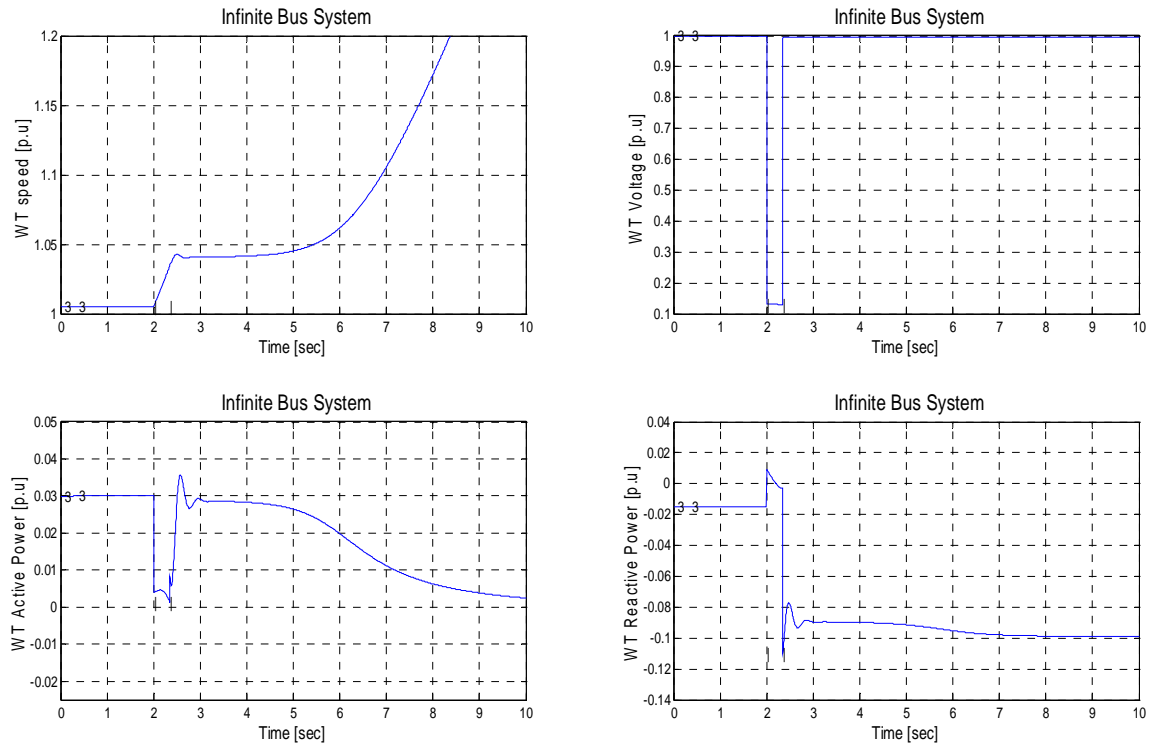


Fig. 4.2b: One mass model transient response with a fault clearing time of 350 ms

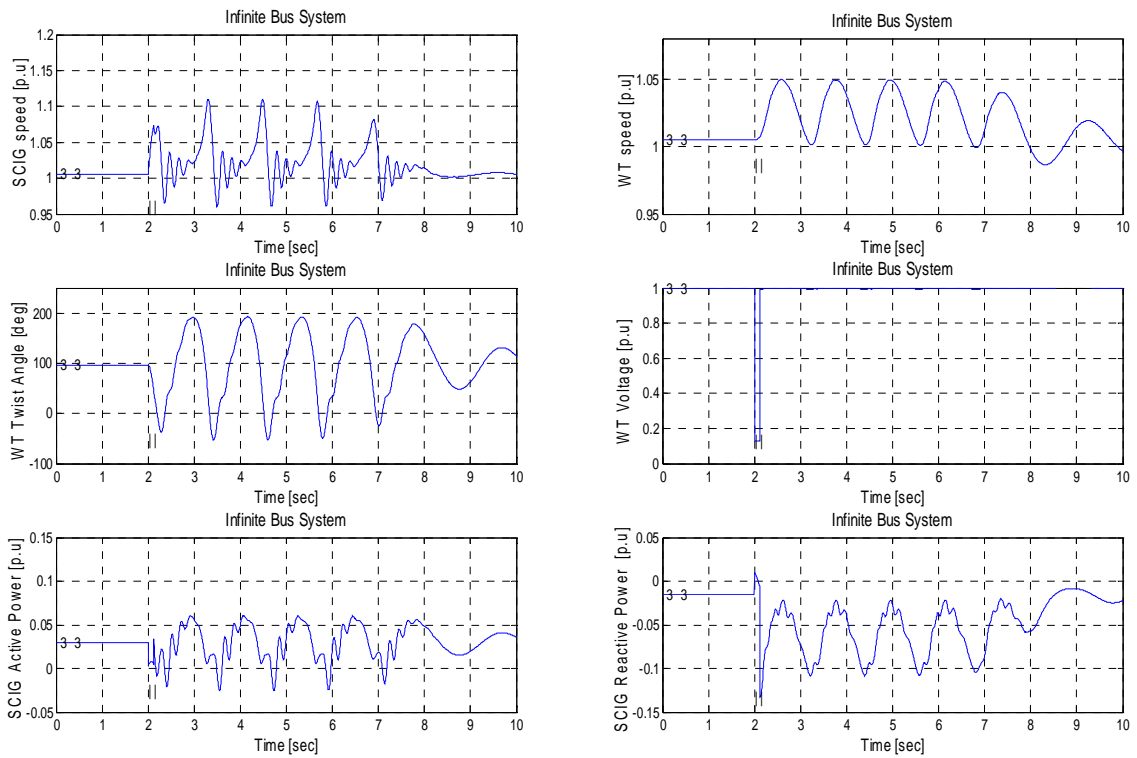


Fig 4.3a: Two mass model transient response with a fault clearing time of 119.23 ms

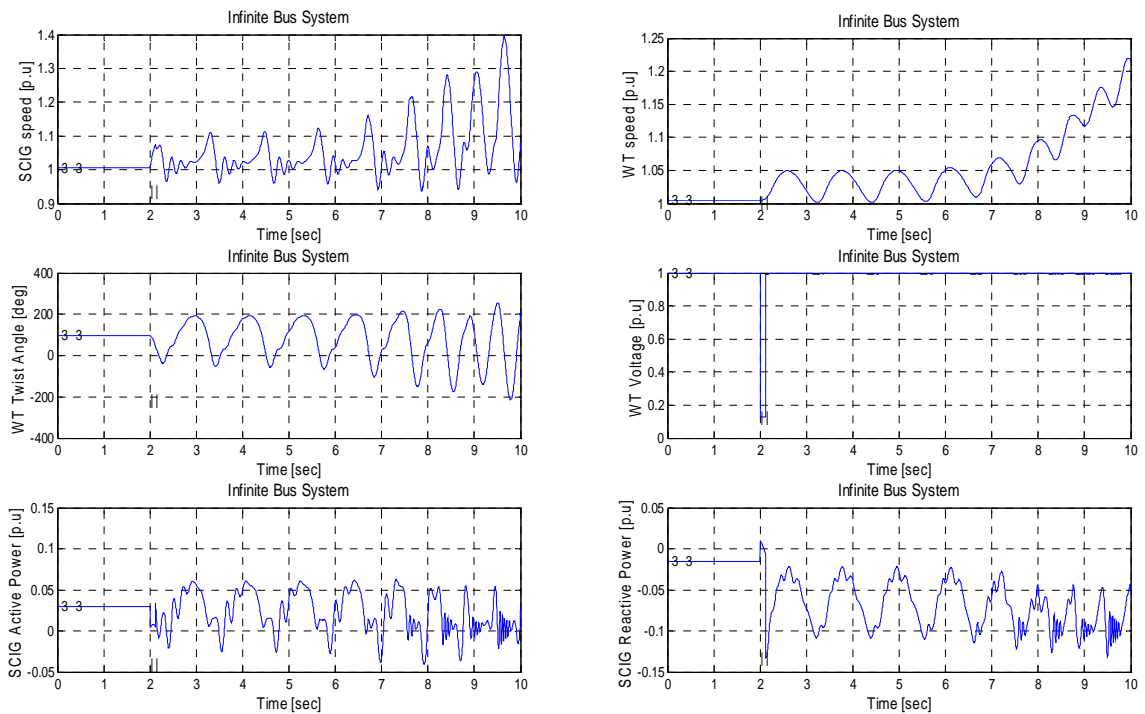


Fig 4.3b: Two mass model transient response with a fault clearing time of 119.28 ms

The shown graphs illustrate the dynamic behavior of a windmill when a three phase fault is applied at its terminals and cleared after a certain interval of time. Figures 4.2a and 4.3a show a stable case as all the variables retain their pre-fault values, while 4.2b and 4.3b reveal an unstable operation. It is apparent that a lumped mass model exhibits fewer oscillations in its operational parameters as compared to a two mass model. The latter experiences perturbations in the SCIG and turbine speeds, the active and reactive powers, and the twist angle. This is attributed to the model itself, where the change in the generator's electromagnetic torque is not only governed by the slip as in the case of a one mass model, but is a function of the turbine's speed and the twist angle. Thus, a shaft model demonstrates the transient behavior of a windmill on the contrary to a lumped mass model, which represents the dynamic behavior of an induction machine. The one mass model also exhibits a much larger critical clearing time (CCT), hence providing a very optimistic assessment of system stability. As a result, its implementation is only favorable when the turbine's data is limited.

The same results have been obtained in [7] with a slight difference in the critical clearing time of the two mass model. The latter remains stable with a fault period extending to 135 milliseconds (ms). The observations of Fig 4.1 are realized in the above plots as well. This can be seen from the increase in the reactive power demand with the increase in slip during the fault period; a fact that may hinder the voltage build-up during the post-fault phase and leads to instability. However, the steady state characteristics of the mentioned figure might not be fairly reliable for the transient analysis, especially when a two mass model is employed. This is expounded with the aid of the following curve:

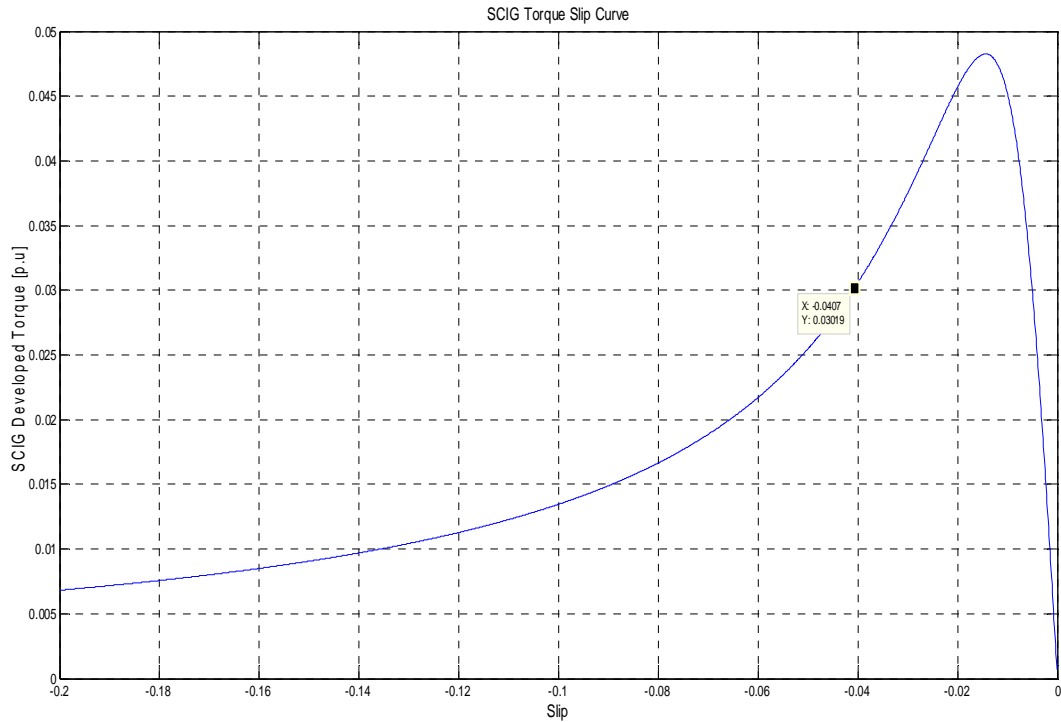


Fig 4.4: 3 MW SCIG torque slip characteristics

Fig 4.4 manifests the torque slip curve of the given SCIG at a post-fault voltage of 0.9955 p.u. The critical slip is defined as the maximum speed that the machine can acquire before losing its stability. Its value at a mechanical input torque (windmill torque) of 0.0302 p.u is -0.0407. Thus, if the generator surpasses this speed, it will accelerate indefinitely. However, this is not the case in both the lumped mass and shaft models. In the former, the turbine reaches a slip of -0.043 and regains its stability (Fig 4. 2a), and in the two mass model the discrepancy is notable. This issue has been addressed in reference [7] to inspect the method of determining the critical clearing time by relying on the critical slip. Researchers have managed to prove its fragility particularly when a two mass model is applied. This is due to the fact that the dynamic performance of an induction machine differs from that of its steady state one, and

depends on the order of the model. The value obtained by the lumped mass model (0.043) for instance appears to be very close, since it incorporates the swing equation of an induction machine, and it only includes the rotor dynamics. If these were set to constant, a first order machine model would result that may appear unstable beyond a slip of -0.0407.

## **4.2 A Case Study on the Lebanese Power System with a Wind Park**

The Lebanese power system contains four major thermal generating plants located along the coastal line of the Mediterranean Sea at Beddawi, Zouk, Jieh, and Zahrani. It also comprises two smaller thermal plants at Baalbeck and Tyre, in addition to a limited number of hydroelectric power plants whose contribution is minor. The thermal units are connected to the 220/150 KV transmission network as depicted by Fig 4.5 hereunder and they are characterized by the following capacities:



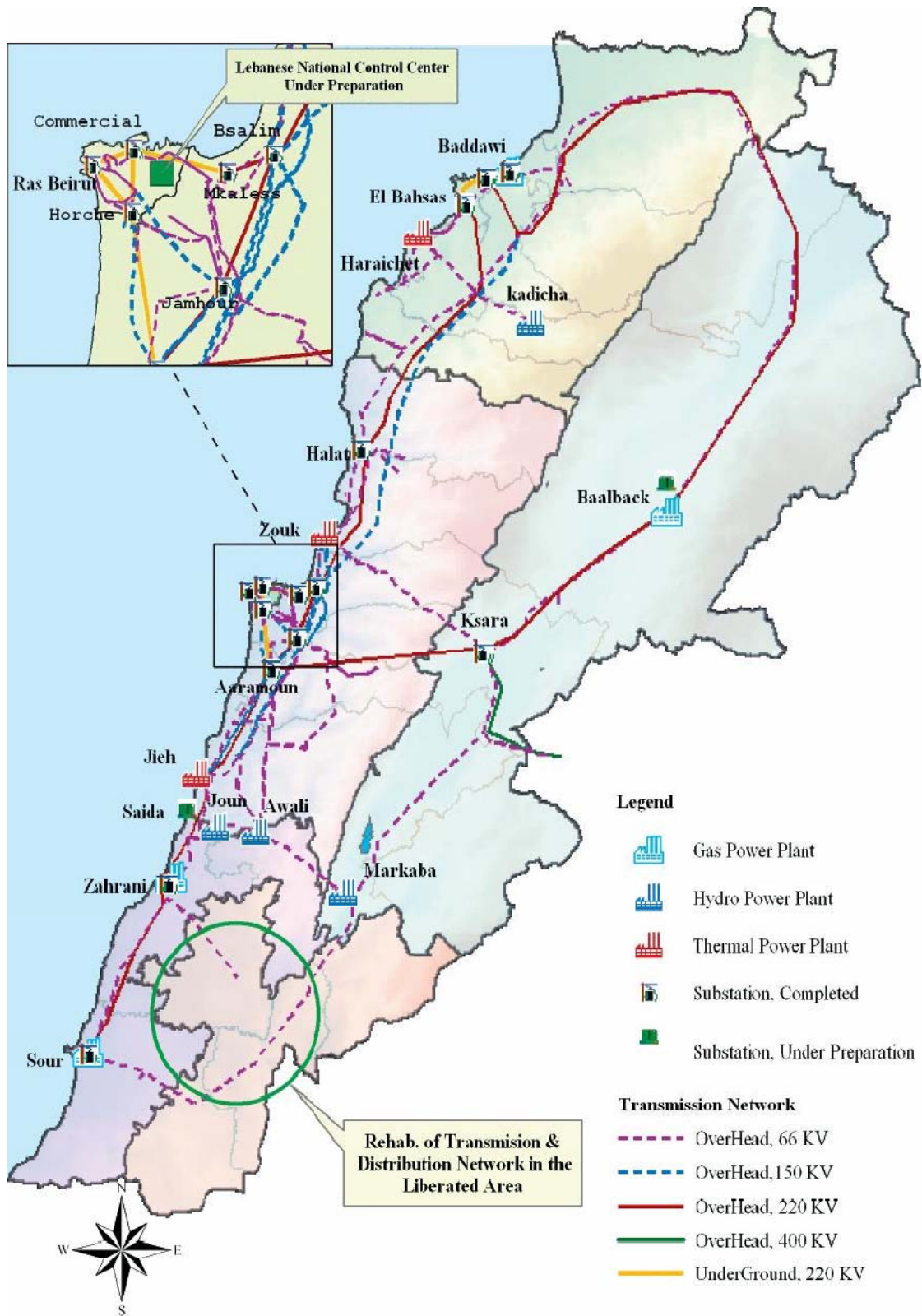


Fig 4.5: The Lebanese power system  
Source: [37]

Table 4.3: Thermal Power Plants in Lebanon

Power Plant	Type	Turbine Rating (MW)	Generator Rating (MVA)
Beddawi	Combined Cycle	415	488
Zouk	Steam Turbine	3*145	3*171
		1*172	1*202
Jieh	Steam Turbine	3*69	3*81
		2*62	2*73
Zahrani	Combined Cycle	415	488
Baalbeck	Combined Cycle	2*35	2*41
Tyre	Combined Cycle	2*35	2*41

A wind farm is expected to be installed in the near future at the northern part of the country in Akkar, and will encompass twenty wind turbines of the Vestas V90-3 MW type [38]. These are 3-bladed pitch regulated units having a rotor diameter of 90 meters (m), and a rated wind speed of 15 meters/second (m/s) [39]. They will spread along a north-south ridge line that tops out at 800 meters high near the town of Machta Hammoud [40], and will supply the 220 KV grid with 60 MW of electricity at the rated wind velocity [38,40]. The latter is most likely achievable at hub heights exceeding 90 meters (m). Table 4.4 below shows the wind data in Akkar at a height of 16m [41].

Table 4.4: Wind Speed Ranges in m/s and Their Probabilities at a Height of 16 m  
Source: [41]

Height (m)	[0, 2[	[2, 6[	[6, 11[	[11, 16[	≥ 16
16	0.197	0.445	0.252	0.08	0.026

The given wind data in Table 4.4 can be converted to a height of 90 m using the following expression [42]:

$$V_{H_2} = V_{H_1} \left( \frac{H_2}{H_1} \right)^x \quad (4.1)$$

Where,  $V_{H_2}$  and  $V_{H_1}$  are the wind speeds at heights  $H_2$  and  $H_1$  respectively. The exponent  $x$  depends on the roughness factor of the ground and is determined based on the work of Counihan (1975) [41-42]] as

$$x = 0.096 \log_{10} z_0 + 0.016 (\log_{10} z_0)^2 + 0.24 \quad (4.2)$$

with

$$0.001 \text{ m} \leq z_0 \leq 10 \text{ m} \quad (4.3)$$

A typical value of  $z_0$  for the region of Akkar seems to be 0.25m, which gives a value of  $x$  equal to 0.188 [41]. By substituting this quantity in equation (4.1), the new wind data will be as follows:

Table 4.5: Wind Speed Ranges in m/s and Their Probabilities at a Height of 90 m

Height (m)	[0, 2.77[	[2.77, 8.3[	[8.3, 15.22[	[15.22, 22.14[	$\geq 22.14$
90	0.197	0.445	0.252	0.08	0.026

A better way to express the wind data of Table 4.5 will be by fitting a probability density function. It is a common practice in wind studies to represent the data by a Weibull distribution. The latter is characterized by its scale parameter  $c$  and its shape parameter  $k$ . These are calculated by statistical procedures such as the moments' method, which in turn relies on both the mean  $\mu$  and the standard deviation  $\sigma$  to estimate the required parameters. Table 4.6 shows the scale and shape parameters

obtained from the average wind speed and the standard deviation deduced from Table 4.5 using standard statistical calculations.

Table 4.6: Weibull Parameters for Akkar at a Height of 90 m

$\mu$	$\sigma$	$c$	$k$
7.77	5.40	8.60	1.48

The accuracy of the values in the table above is confirmed by MATLAB, and the plot of the corresponding Weibull distribution is as shown in Fig 4.6 below:

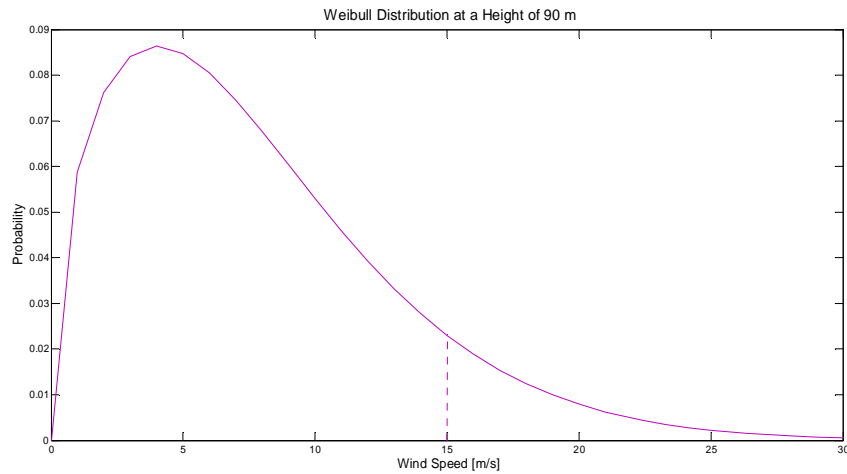


Fig 4.6: Weibull distribution for Akkar at a height of 90 m

It is obvious from the displayed plot that there is an appreciable probability (0.1025) that the wind speed transcends 15 m/sec, and hence it becomes important to study the transient stability of the Lebanese network with 60 MW of wind power. The study can be performed at a lower penetration level such that the turbines operate at a lower speed, however the critical clearing time will acquire a larger value due to the increase in the critical slip with the reduction of the input wind torque.

In this section, a case study on the 220/150 KV Lebanese network will be conducted to analyze the transient stability of the system upon the integration of the described wind farm. Certain assumptions have been made to account for the deficiencies in the wind park data. Thus, each windmill has been considered to be equipped with a step-up transformer that links it to a 34.5 KV substation. The latter would raise the voltage level to 220 KV and supply the generated wind power through an overhead double circuit transmission line, which extends from the town of Machta Hammoud to Beddawi.

#### 4.2.1 Simulation Model and Results

A single line diagram of the 220/150 KV Lebanese network is displayed by the figure below:

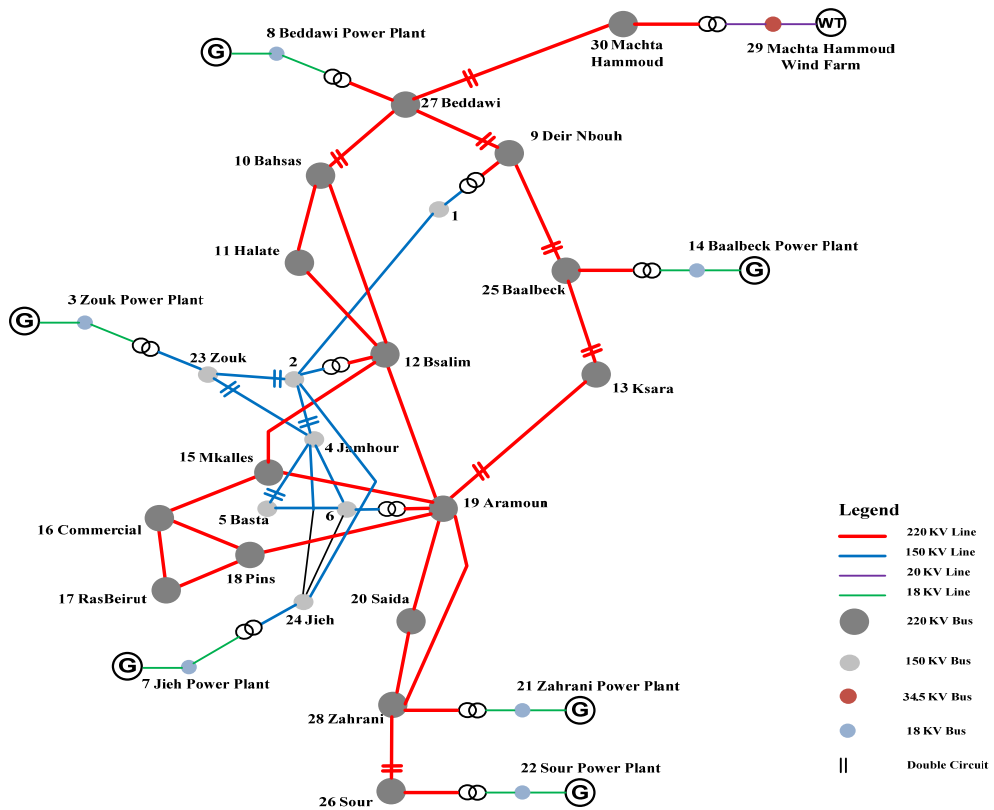


Fig 4.7: One Line Diagram of the 150/220 KV transmission network with bus numbers

The system has 30 bus bars, 33 transmission lines, 10 transformers, 6 conventional power plants, and a wind farm. Each power plant is modeled by one equivalent generator whose rating is the aggregate of the entire units. This model is adopted because the machines are connected to the same bus and their rotors swing coherently. The turbines in the wind park are also represented by one equivalent machine as discussed earlier in Chapter 3. Every individual windmill employs the SCIG of Table 4.2 with the reactances scaled down to 50 Hz. The combined transformer reactance of all the turbines is lumped with the substation transformer (34.5/220 KV). Regarding the rating of a power plant equivalent; this is determined as follows:

- Find the average rating  $R$  of  $n$  machines in a given power plant.
- Assume that the plant is made up of  $n$  identical machines rated  $R$ .
- Example: Jieh power plant would have 5 identical units of 77.8 MVA.

This method of equivalency is approximate. It is implemented due to the deficiency in the generator data of Table 4.3. The data of the chosen synchronous machines and that of the lines, the transformers and the loads is presented in the appendix.

In this simulation, three cases involving three phase faults in the vicinity of the wind farm are investigated. These inspect the stability of the synchronous machines upon the loss of wind power, and the critical clearing time (CCT) variation with:

- The reactive power compensation at the terminals of the wind farm.
- The fault location.
- The penetration level of wind power

The fault is created at  $t=2.0$  seconds and the transient response of the system is depicted by the subsequent figures.

### 4.2.1.1 Case 1

In this case a symmetrical fault is applied at bus 29 and the effect of adding a capacitor bank at this bus during the pre-fault conditions is noted:

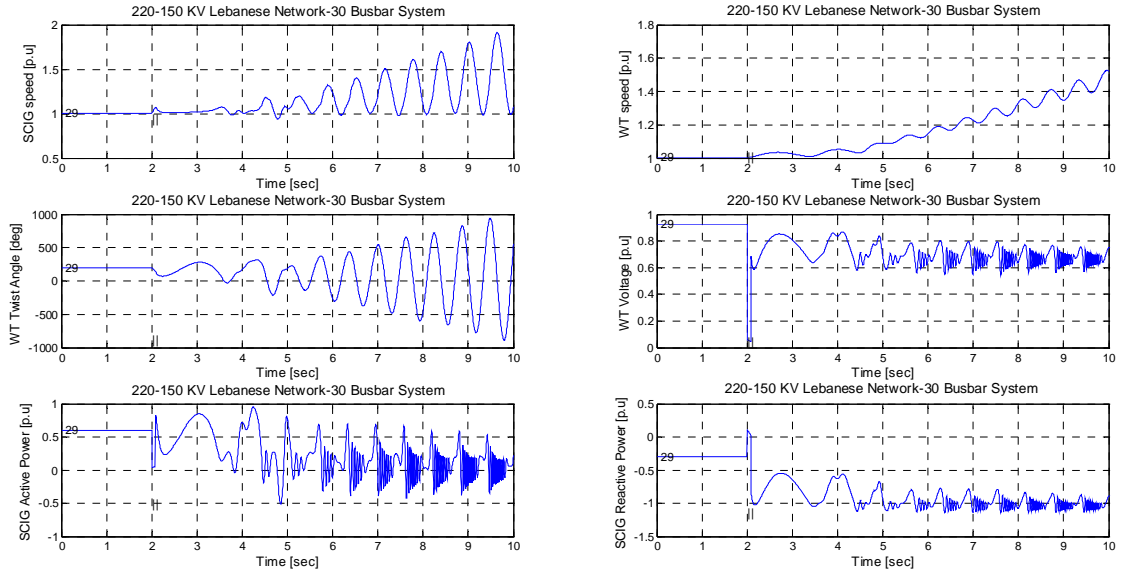


Fig 4.8a: Wind farm transient response without a capacitor bank. CT: 84 ms

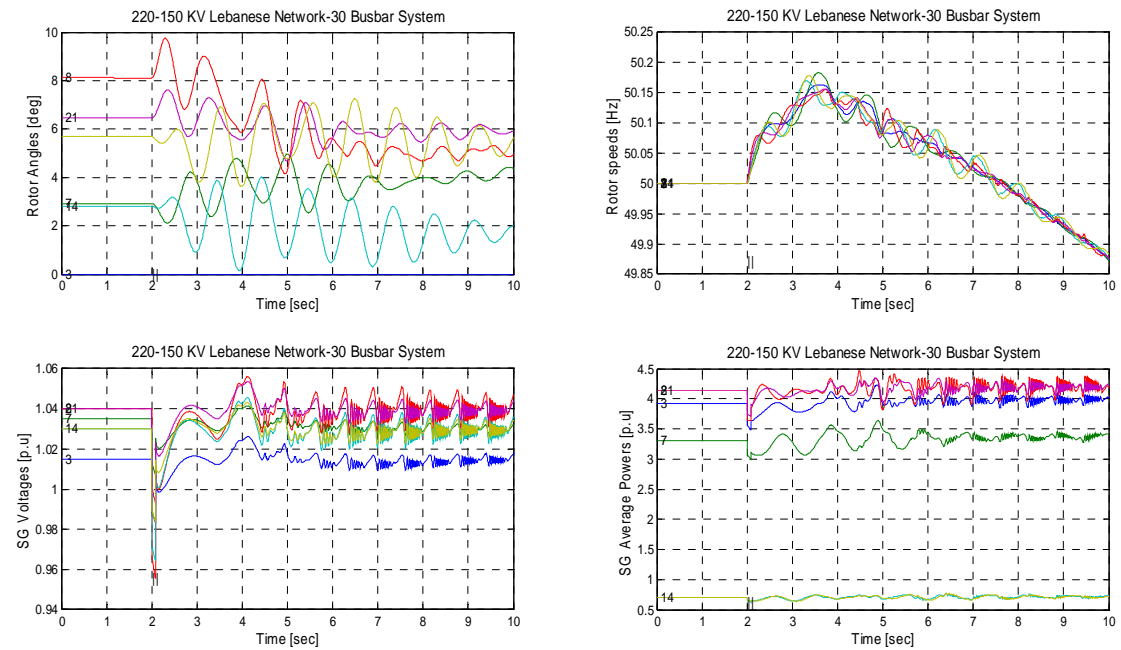


Fig 4.8b: Synchronous machines transient response without a capacitor bank. CT: 84 ms

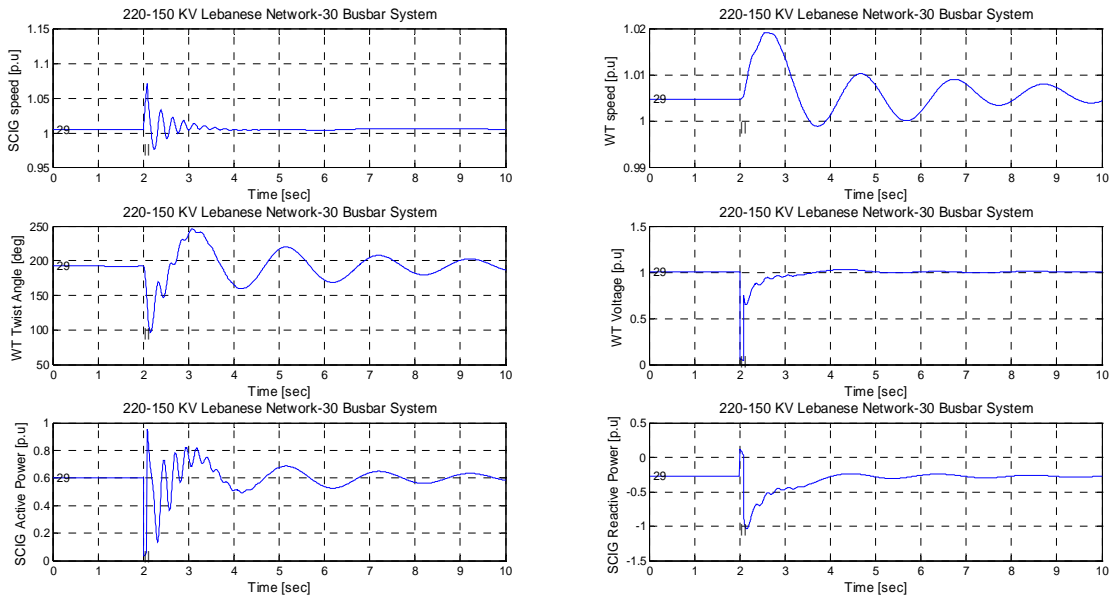


Fig 4.9a: Wind farm transient response with a capacitor bank. CT: 84 ms

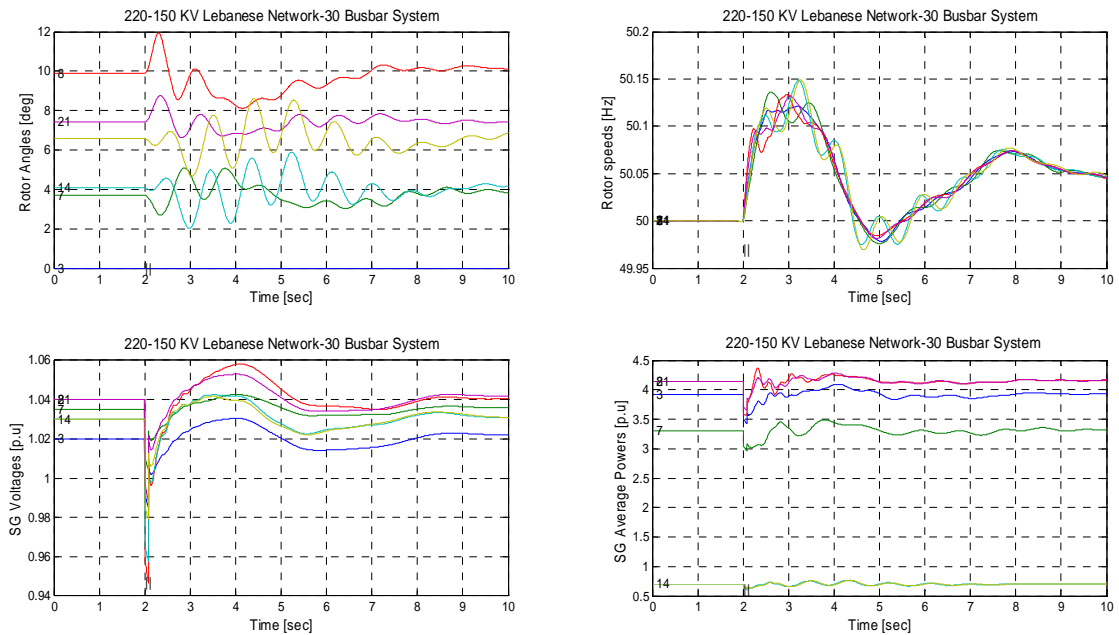


Fig 4.9b: Synchronous machines transient response with a capacitor bank. CT: 84 ms

The significance of the power factor at the wind farm terminals is demonstrated in this case. Fig 4.8 shows an unstable system response at a clearing time of 84 ms. The



turbines cease to generate active power as a result of the indefinite increase in slip and they only consume reactive power. The system frequency also drops due to the loss of wind power Fig 4.8b, which in turn is compensated by the synchronous machines. A governor model is not implemented in this work, thus the mechanical input power remains constant and the increase in the air gap power triggers a further drop of speed. The purpose of a shunt capacitor is to fully supply the reactive power demand of the windmills and raise the voltage at their terminals. This affects the slip, where its initial value will decrease and its critical one will increase, hence yielding a more stable behavior. The capacitor has been designed such that it produces a unity power factor at the wind farm terminals. The magnitude of its reactance  $X_c$  is equal to one third of the magnetizing reactance of the SCIG. Thus, for  $n$  wind turbines, an equivalent capacitive reactance of  $\frac{X_L}{3n}$  would be installed. Fig 4.9a displays its influence on the critical clearing time (CCT), where the system looks stable beyond a fault period of 84 ms. It is recognized that the SCIG and turbine speeds regain their initial values after the disturbance. The active and reactive power levels also recover together with the terminal voltage. Concerning the synchronous machines in Fig 4.9b, they are hardly affected by the disturbance and this can be seen from their swing curves. The rotor angles and speeds undergo an under-damped oscillatory response and eventually return to their initial values. The active power generation is restored as well, and the loads are continuously supplied. Beddawi power plant seems to be mostly affected by the fault since it is the closest to the wind farm, and it suffers from the largest voltage drop among the other sets (0.94 p.u). The impact of the AVR system is also realized through the voltage plots, which eventually regain their initial values.

#### 4.2.1.2 Case 2

The objective of this case is to confirm that a three phase fault at the wind farm terminals will be the most severe. The critical clearing time is expected to increase with a distant fault location. This is illustrated by the following figure, which portrays the transient response of the wind farm upon a fault applied near bus 27 and isolated by removing one circuit of the transmission line joining Beddawi with Bahsas (27-10).

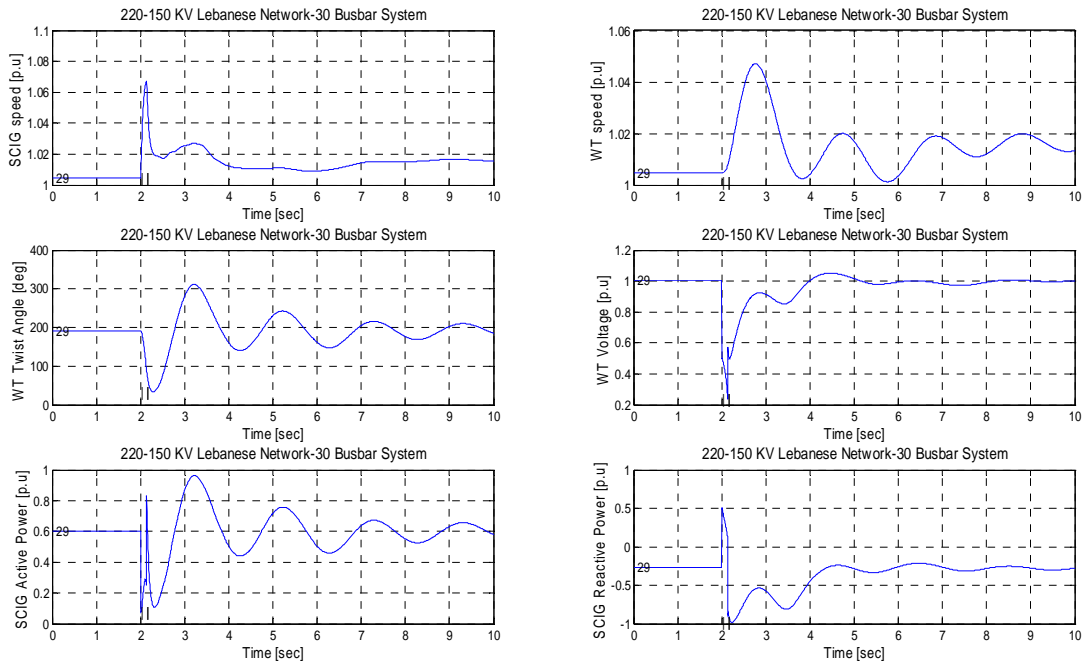


Fig 4.10: Wind farm transient response with a capacitor bank. CCT: 140 ms

Fig 4.10 depicts the transient response of the wind park during the described fault. The voltage, speed, and power variations are similar to those of the previous case due to the model that describes the machine's dynamic behavior. This also applies to the synchronous machines. However, the critical clearing time is now higher and it reaches 140 ms, whereas it has been limited to 96 ms in Case 1.

### 4.2.1.3 Case 3

In this case the wind penetration level is being increased to 99 MW representing 33 windmills at the farm. The disturbance of the previous case is simulated and the results are shown in Fig. 4.11.:

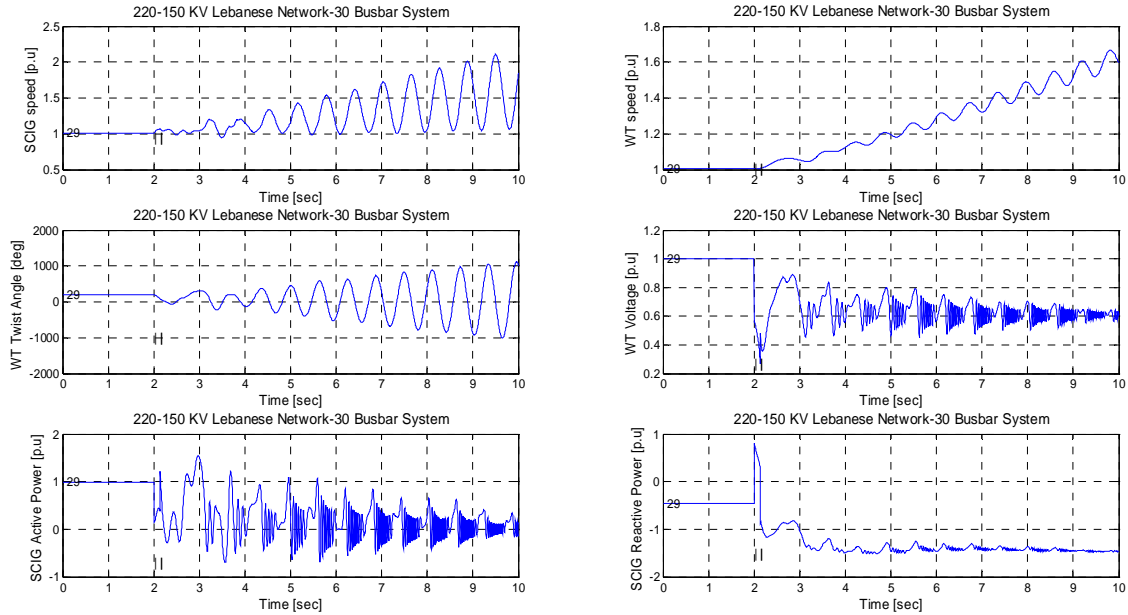


Fig 4.11a: Wind farm transient response with a capacitor bank. CT: 140 ms

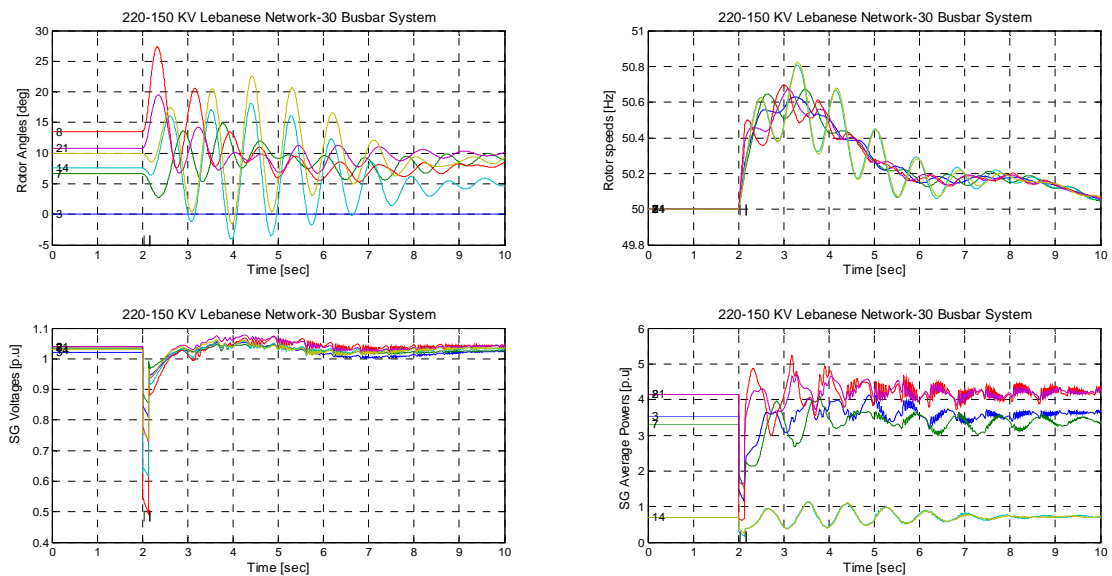


Fig 4.11b: Synchronous machines transient response with a capacitor bank. CT: 140 ms

The figures above illustrate the transient response of the system at a clearing time of 140 ms. The wind park is unstable as a result of the increased penetration of wind power. This is attributed to the amplified reactive power consumption during the transient period, which prevents the voltage recovery at the given fault duration. For the same number of turbines (i.e. 33) when the output is reduced to 2 MW per turbine, the system becomes more stable; the CCT becomes 799 ms instead of 125 ms. This is attributed to the considerable increase in the critical slip.

With regard to the synchronous machines, it is obvious that the Beddawi generating set suffers the most because of its location. The system frequency follows a relatively decreasing trend as the machines try to compensate for the missing portion of wind power. This is portrayed by Fig 4.11b, as the power plants increment their generation except for Baalbeck and Tyre that represent the smallest sets in the system, and are far from the fault location. The decline in speed is due again to the lack of a governor model, which results in a constant mechanical input power that cannot be made to match the electric power required by the network.

### **4.3 Summary**

The validity of the proposed methodologies for solving the load flow and transient stability problems is established in this chapter. Two test systems are utilized for this purpose and the obtained results prove to be consistent. The transient stability program is used further to evaluate the stability of the 220/150 KV Lebanese network with a grid-connected wind farm.

## CHAPTER 5

### CONCLUSIONS AND FUTURE WORK

In this thesis, the transient stability of fixed speed wind turbines is examined for severe network disturbances. A load flow algorithm is primarily highlighted to demonstrate the interaction of a wind farm with the grid, and provide the necessary initial conditions for the transient stability problem. The machine dynamic models are presented together with their comprehensive initialization and integration techniques. These are incorporated in a transient stability program, which is written in MATLAB and used to carry out a case study on the 220/150 KV Lebanese network with an integrated wind park. The validity of this program is verified by comparing its results with those of a given reference that uses an infinite bus test system. Results show that a one mass model yields an optimistic assessment for the transient stability of windmills and it doesn't accurately describe the dynamic behavior. For these reasons, a shaft model with two masses is always favored as it models the oscillatory response in a precise manner. This is used in the simulations of the Lebanese network, which show that a disturbance near the wind farm will have a minor effect on the whole system since the portion of wind power remains small as compared to the total amount of generation. The transient stability of the connected wind farm is improved with reactive power compensation. However, an increased penetration level along with a close fault location can significantly deteriorate its stability. This is due to the lack of control on the terminal voltage of a SCIG, and to the absence of a pitch controller, which may play an important role in limiting the turbine's speed in the fault period.

The current work can be further improved by adding the speed governing models, which include a pitch controller and a governor. The former represents the only means of control for a fixed speed wind generating unit along with static VAR compensation. An SVC regulator can supply the wind turbines with the required reactive power during the fault period, since it is voltage controlled. This makes up for the lack of steady state VARs during the fault as they are proportional to the square of the voltage and hence reflects positively on the terminal voltage and aid its recovery.

## APPENDIX 1

### LINE AND MACHINE DATA

The following table includes the branch data of the simulated system in 4.2.1.

The values are in per unit on a 100 MVA system base:

220 KV Overhead Transmission Lines							
From	To	Km	R	X	Y	MW	Circuits
27	9	12	0.00146	0.00962	0.01931	360	2
27	10	12	0.00080	0.00429	0.50704	375	2
10	12	65	0.00396	0.03868	0.13320	720	1
10	11	45	0.00274	0.02678	0.09222	720	1
11	12	20	0.00122	0.01190	0.04099	720	1
12	15	9	0.00109	0.00721	0.01448	360	1
15	19	14	0.00170	0.01122	0.02253	360	1
12	19	22	0.00134	0.01309	0.04508	720	1
19	20	30	0.00183	0.01785	0.06148	720	1
19	28	38	0.00232	0.02261	0.07787	720	1
20	28	8	0.00049	0.00476	0.01639	720	1
28	26	34	0.00562	0.02726	0.05472	270	2
19	13	48	0.00583	0.03848	0.07725	360	2
25	13	40	0.00486	0.03207	0.06437	360	2
25	9	80	0.00972	0.06413	0.12874	360	2
15	16	9	0.00095	0.00344	0.38028	210	1
16	17	4	0.00042	0.00153	0.16901	210	1
17	18	4	0.00042	0.00153	0.16901	210	1
16	18	5	0.00053	0.00191	0.21127	210	1
18	19	14	0.00148	0.00535	0.59154	210	1
150 KV Overhead Transmission Lines							
2	1	63.8	0.02268	0.11002	0.04737	184	1
2	23	8.5	0.00151	0.01077	0.00819	368	2
4	23	17.5	0.00311	0.02217	0.01685	368	2
4	2	11.8	0.00420	0.02035	0.00876	184	2
4	24	26.3	0.00935	0.04535	0.01953	184	1
2	24	36.6	0.01301	0.06311	0.02718	184	1
6	24	17.5	0.00622	0.03018	0.01299	184	1
6	4	8.8	0.00313	0.01518	0.00653	184	1
4	5	11.1	0.00333	0.00957	0.21803	150	2
6	5	16	0.00481	0.01380	0.31428	150	1

<b>220/150 KV Transformers</b>							
6	19			0.125		100	2
1	9			0.125		100	2
2	12			0.125		100	2
<b>Power Plant Equivalent Transformers</b>							
3	23			0.01784		715	1
7	24			0.03213		389	1
14	25			0.15245		82	1
22	26			0.15245		82	1
8	27			0.02560		488	1
21	28			0.02560		488	1
<b>Machta Hammoud-Beddawi 220 KV Transmission Line</b>							
30	27	60	0.0073	0.00481	0.0966	360	2
<b>Individual Windmill Transformer</b>							
				1.4		5	1
<b>60 MW Wind Farm Equivalent Transformer</b>							
29	30			0.1742		120	1
<b>Three Phase Fault Reactance</b>							
0.01							

The load data is shown in the Table below. All the values in this table have been multiplied by a factor of 0.75, since the total load exceeds the generation capacity:

<b>Node</b>	<b>P (MW)</b>	<b>Q (MVar)</b>	<b>Node</b>	<b>P (MW)</b>	<b>Q (MVar)</b>
1	82	51	12	70	43
2	46	29	13	163	101
23	132	82	25	94	58
4	240	149	15	66	41
5	233	145	16	122	75
6	46	29	17	93	58
24	60	37	18	75	46
27	44	28	19	86	53
9	51	31	20	110	68
10	221	137	28	161	100
11	35	22	26	98	60



The following table contains the synchronous machine data that is necessary for the transient analysis. The values are in per unit on a 100 MVA system base:

Source: [43]

<b>Synchronous Machine Data</b>						
<b>Plant</b>	Zouk	Jieh	Baddawi	Baalbeck	Zahrani	Sour
<b>Units MVA</b>	4*178.75	5*77.8	3*162.67	2*41	3*162.67	2*41
<b><math>R</math></b>	0.000364	0.000797	0.000635	0.0017	0.000635	0.0017
<b><math>X_d</math></b>	0.2309	0.2699	0.3484	1.7073	0.3484	1.7073
<b><math>X'_d</math></b>	0.0324	0.0476	0.0502	0.2817	0.0502	0.2817
<b><math>X_q</math></b>	0.2224	0.2519	0.3361	1.6732	0.3361	1.6732
<b><math>X'_q</math></b>	0.0531	0.0925	0.0779	0.872	0.0779	0.872
<b><math>T'_{d0}</math></b>	5.9	6.1	5.9	5.5	5.9	5.5
<b><math>T'_{q0}</math></b>	0.535	0.3	0.54	1.5	0.54	1.5
<b><math>H</math></b>	26.36	23.2	19.02	3.6	19.02	3.6
<b>Exciter Data</b>						
<b><math>T_R</math></b>	0.06	0.06	0.06	0.06	0.06	0.06
<b><math>T_A</math></b>	0.2	20	0.2	0.05	0.2	0.05
<b><math>T_E</math></b>	0.5685	1.98	0.56	0.5	0.56	0.5
<b><math>T_F</math></b>	0.35	1.00	0.35	1.00	0.35	1.00
<b><math>K_A</math></b>	25	0.05	25	57.14	25	57.14
<b><math>K_E</math></b>	-0.0505	1.00	-0.0497	-0.0445	-0.0497	-0.0445
<b><math>K_F</math></b>	0.091	0.08	0.0896	0.08	0.0896	0.08
<b><math>S_{75}</math></b>	0.0778	0.0967	0.0765	0.0684	0.0765	0.0684
<b><math>S_{100}</math></b>	0.303	0.3774	0.2985	0.2667	0.2985	0.2667
<b><math>E_{fmax}</math></b>	3.96	3.18	4.02	4.5	4.02	4.5
<b><math>V_{RMIN}</math></b>	-1.0	0.0	-1.0	-1.0	-1.0	-1.0
<b><math>V_{RMAX}</math></b>	1.0	4.38	1.0	1.0	1.0	1.0

## BIBLIOGRAPHY

- [1] Bahramipanah, Maryam, Saeed Afsharnia, and Zagros Shahooei. "A survey on the effect of different kinds of wind turbines on power system stability." In *Nuclear & Renewable Energy Conference (INREC), 2010 1st International*, pp. 1-6. IEEE, 2010.
- [2] Ofualagba, G., and E. U. Ubeku. "Wind energy conversion system-wind turbine modeling." In *Power and Energy Society General Meeting-Conversion and Delivery of Electrical Energy in the 21st Century, 2008 IEEE*, pp. 1-8. IEEE, 2008.
- [3] Muyeen, S. M., M. Hasan Ali, R. Takahashi, T. Murata, J. Tamura, Y. Tomaki, A. Sakahara, and E. Sasano. "Comparative study on transient stability analysis of wind turbine generator system using different drive train models." *Renewable Power Generation, IET* 1, no. 2 (2007): 131-141.
- [4] Salman, Salman K., and Anita LJ Teo. "Windmill modeling consideration and factors influencing the stability of a grid-connected wind power-based embedded generator." *Power Systems, IEEE Transactions on* 18, no. 2 (2003): 793-802.
- [5] Li, Hui, and Zhe Chen. "Transient stability analysis of wind turbines with induction generators considering blades and shaft flexibility." In *Industrial Electronics Society, 2007. IECON 2007. 33rd Annual Conference of the IEEE*, pp. 1604-1609. IEEE, 2007.
- [6] Li, H., B. Zhao, C. Yang, H. W. Chen, and Z. Chen. "Analysis and estimation of transient stability for a grid-connected wind turbine with induction generator." *Renewable Energy* 36, no. 5 (2011): 1469-1476.
- [7] Li, Hui, Zhe Chen, and L. Han. "Comparison and evaluation of induction generator models in wind turbine systems for transient stability of power system." In *Power System Technology, 2006. PowerCon 2006. International Conference on*, pp. 1-6. IEEE, 2006.
- [8] Jurado, Alejandro, and Mario Brugnioni. "The effect of fixed speed wind turbines models on transient stability of power system." In *Electricity Distribution-Part 1, 2009. CIRED 2009. 20th International Conference and Exhibition on*, pp. 1-4. IET, 2009.
- [9] Ledesma, P., J. Usaola, and J. L. Rodriguez. "Transient stability of a fixed speed wind farm." *Renewable energy* 28, no. 9 (2003): 1341-1355.
- [10] Li, Shenghu, Zhengkai Liu, Xinjie Hao, and Shusen Jia. "Dynamic equivalence to induction generators and wind turbines for power system stability analysis." In *Power Electronics for Distributed Generation Systems (PEDG), 2010 2nd IEEE International Symposium on*, pp. 887-892. IEEE, 2010.

- [11] Qiao, Wei, Ronald G. Harley, and Ganesh K. Venayagamoorthy. "Dynamic modeling of wind farms with fixed-speed wind turbine generators." In *Power Engineering Society General Meeting, 2007. IEEE*, pp. 1-8. IEEE, 2007.
- [12] Fernández, Luis M., José Ramón Saenz, and Francisco Jurado. "Dynamic models of wind farms with fixed speed wind turbines." *Renewable Energy* 31, no. 8 (2006): 1203-1230.
- [13] Trudnowski, Daniel J., Andrew Gentile, Jawad M. Khan, and Eric M. Petritz. "Fixed-speed wind-generator and wind-park modeling for transient stability studies." *Power Systems, IEEE Transactions on* 19, no. 4 (2004): 1911-1917.
- [14] El-Shimy, M., M. A. L. Badr, and O. M. Rassem. "Impact of large scale wind power on power system stability." In *Power System Conference, 2008. MEPCON 2008. 12th International Middle-East*, pp. 630-636. IEEE, 2008..
- [15] Chen, Zhe, Y. Hu, and Frede Blaabjerg. "Stability improvement of induction generator-based wind turbine systems." *Renewable Power Generation, IET* 1, no. 1 (2007): 81-93.
- [16] Salman, S. K., and A. L. J. Teo. "Improvement of fault clearing time of wind farm using reactive power compensation." In *Power Tech Proceedings, 2001 IEEE Porto*, vol. 2, pp. 6-pp. IEEE, 2001.
- [17] Tamura, J., T. Yamazaki, R. Takahashi, S. Yonaga, Y. Matsumura, and H. Kubo. "Simulation analyses of transient stability of wind generators." *International journal of power & energy systems* 27, no. 2 (2007): 131-139.
- [18] Ledesma, Pablo, and Julio Usaola. "Doubly fed induction generator model for transient stability analysis." *Energy conversion, iee transactions on* 20, no. 2 (2005): 388-397.
- [19] Ekanayake, Janaka B., Lee Holdsworth, XueGuang Wu, and Nicholas Jenkins. "Dynamic modeling of doubly fed induction generator wind turbines." *Power Systems, IEEE Transactions on* 18, no. 2 (2003): 803-809.
- [20] Poller, Markus A. "Doubly-fed induction machine models for stability assessment of wind farms." In *Power Tech Conference Proceedings, 2003 IEEE Bologna*, vol. 3, pp. 6-pp. IEEE, 2003.
- [21] Bufano, V., M. Dicorato, A. Minoia, and M. Trovato. "Embedding wind farm generation in power system transient stability analysis." In *Power Tech, 2005 IEEE Russia*, pp. 1-7. IEEE, 2005.
- [22] Usaola, Julio, Pablo Ledesma, J. M. Rodriguez, J. L. Fernandez, D. Beato, R. Iturbe, and J. R. Wilhelmi. "Transient stability studies in grids with great wind power penetration. Modelling issues and operation requirements." In *Power Engineering Society General Meeting, 2003, IEEE*, vol. 3. IEEE, 2003.

- [23] Holdsworth, L., X. G. Wu, J. B. Ekanayake, and N. Jenkins. "Comparison of fixed speed and doubly-fed induction wind turbines during power system disturbances." In *Generation, Transmission and Distribution, IEE Proceedings-*, vol. 150, no. 3, pp. 343-352. IET, 2003.
- [24] Martin, Kaltschmitt, Streicher Wolfgang, and Wiese Andreas. "Renewable Energy: Technology, Economics and Environment." PhD diss., Springer, 2007.
- [25] Manwell, James F., Jon G. McGowan, and Anthony L. Rogers. "Wind energy explained: theory, design and application. 2002." *John Wiley&Sons Ltd, UK*(2002): 577.
- [26] Nunes, M. V. A., U. H. Bezerra, and H. H. Zurn. "Transient stability margin of variable versus fixed speed wind systems in electrical grids." In *Power Tech Conference Proceedings, 2003 IEEE Bologna*, vol. 3, pp. 7-pp. IEEE, 2003.
- [27] Feijoo, A. E., and Cidras. J. "Modeling of wind farms in the load flow analysis." *Power Systems, IEEE Transactions on* 15, no. 1 (2000): 110-115.
- [28] Fuerte-Esquivel, C.R., Tovar-Hernandez, J.H., Gutierrez-Alcaraz, G., Cisneros-Torres, F., Feijoo, A.E., and Cidras, J., "Discussion of "Modeling of wind farms in the load flow analysis"", *IEEE Transactions on Power Systems*, vol. 16, no. 4, Nov. 2001, pp. 951 -952.
- [29] Divya, K. C., and P. S. Rao. "Models for wind turbine generating systems and their application in load flow studies." *Electric Power Systems Research* 76, no. 9 (2006): 844-856.
- [30] Liu, Yanni, Wei Wang, Lijie Xu, Pinghao Ni, and Lin Wang. "Research on power flow algorithm for power system including wind farm." In *Electrical Machines and Systems, 2008. ICEMS 2008. International Conference on*, pp. 2551-2555. IEEE, 2008.
- [31] Feijóo, Andrés. "On PQ models for asynchronous wind turbines." *Power Systems, IEEE Transactions on* 24, no. 4 (2009): 1890-1891.
- [32] Stevenson, William D., and John J. Grainger. "Power system analysis." *Nova Iorque: McGraw-Hill International Editions* , 1994.
- [33] M. Pavella, P.G. Murthy. "Transient Stability of Power Systems." Wiley, New York, 1994
- [34] Arrillaga and Arnold, 1990 J. Arrillaga, C.P. Arnold. "Computer Analysis of Power Systems." Wiley, Chichester , 1990
- [35] Set, Emergency Generator. "Computer Representation of Excitation Systems." (1967).

- [36] Sloomweg, Johannes Gerlof. "Wind power: Modeling and impact on power system dynamics." PhD diss., 2003.
- [37] Abi Ali, Nadim Amal "Investigation of the stability of a distributed generation plan for the Lebanese power system." Thesis, American University of Beirut, 2007.
- [38] <http://www.butec.com.lb/projectDetails.aspx?CategoryID=5&ProjectID=152&SubID=36>
- [39 ] <http://www.vestas.com>
- [40] <http://www.executive-magazine.com/real-estate-and-development/First-sails-to-the-wind/4936>
- [41] A.Kronfol, R.Zahr, S.Hawi, "Renewable Energy System in Lebanon", Final Year Project, American University of Beirut, 2010.
- [42] S.N. Bhadra, D. Kashta & S. Banerjee, *Wind Electrical Systems*, New Delhi: Oxford University Press, 2004.
- [43] Anderson, Paul M., and Aziz A. Fouad. "Power system control and stability. " John Wiley & Sons, 2008.

